Pontifícia Universidade Católica
do Rio de Janeiro

Matheus Patrick Soares Barbosa

Nonlinear Black-box Identification of Piezoelectric Systems

Dissertação de Mestrado

Dissertation presented to the Programa de Pós–graduação em Engenharia Mecânica of PUC-Rio in partial fulfillment of the requirements for the degree of Mestre em Engenharia Mecânica.

Advisor: Prof. Helon Vicente Hultmann Ayala

Rio de Janeiro
April 2021

Pontifícia Universidade Católica
do Rio de Janeiro

Matheus Patrick Soares Barbosa

Nonlinear Black-box Identification of Piezoelectric Systems

Dissertation presented to the Programa de Pós–graduação em Engenharia Mecânica of PUC-Rio in partial fulfillment of the requirements for the degree of Mestre em Engenharia Mecânica. Approved by the Examination Committee:

Prof. Helon Vicente Hultmann Ayala
Advisor
Departamento de Engenharia Mecânica – PUC-Rio

Prof. Arthur Martins Barbosa Braga
Departamento de Engenharia Mecânica - PUC-Rio

Prof. Alan Conci Kubrusly
Centro de Estudos em Telecomunicações - PUC-Rio

Rio de Janeiro, April the 26th, 2021

Matheus Patrick Soares Barbosa

Licensed Technician, in 2011, and Mechanical Engineer, in 2016, both from the Federal Center for Technological Education Celso Suckow da Fonseca (CEFET/RJ).

Bibliographic data

Barbosa, Matheus Patrick Soares

Nonlinear Black-box Identification of Piezoelectric Systems / Matheus Patrick Soares Barbosa; advisor: Helon Vicente Hultmann Ayala. – 2021.

84 f: il. color. ; 30 cm

Dissertação (mestrado) - Pontifícia Universidade Católica do Rio de Janeiro, Departamento de Engenharia Mecânica, 2021.

Inclui bibliografia

1. Engenharia Mecânica – Teses. 2. Atuadores piezoelétricos. 3. Identificação de sistema não lineares. 4. Métodos de identificação e controle. 5. Micromanipuladores piezoelétricos. 6. Modelagem Caixa Preta . I. Ayala, Helon Vicente Hultmann. II. Pontifícia Universidade Católica do Rio de Janeiro. Departamento de Engenharia Mecânica. III. Título.

CDD: 621

Acknowledgments

To my advisor Prof. Helon Vicente for the continuous stimulus to improve this work. I am very grateful for his partnership.

To my parents for their education, attention, and affection at all times, even in the most difficult moments.

To my girlfriend Priscila Coelho for her fundamental support in crucial moments and inspiration to always improve.

To the engineers and colleagues Murilo Camerini, Carla Kato, Roberth Llerena, Bruno Sapha, Leone Masiero, and Bruno Leão for their important contributions made to my development as a professional.

To Prof. Arthur Braga from PUC-Rio for his encouragement to be part of the program and support in improving my career.

To my colleagues at PUC-Rio Walisson, Estelio, Renata, and Thiagos for the support given during the program.

To my colleague Daniel Pereira for his great help during the acquisition of data for the models presented here and partnership in the publications made.

To colleagues at the Laboratório de Sensores de Fibra Ótica (LSFO) at PUC-Rio, for the time and equipments for data acquisition.

To the professors Alan Conci Kubrusly, Arthur Martins Barbosa Braga, and Igor Braga de Paula from PUC-Rio who made themselves available to participate in the Examination Committee.

To all the professors and employees of the Mechanical Engineering Department who helped me in times of doubt.

To all the friends and family who, in one way or another, stimulated or helped me. Special thanks to Álvaro Florentino for his friendship all these years.

This study was financed in part by the Coordenação de Aperfeiçoamento de Pessoal de Nível Superior - Brasil (CAPES) - Finance Code 001

Abstract

Barbosa, Matheus Patrick Soares; Ayala, Helon Vicente Hultmann (Advisor). **Nonlinear Black-box Identification of Piezoelectric Systems**. Rio de Janeiro, 2021. 84p. Dissertação de Mestrado – Departamento de Engenharia Mecânica, Pontifícia Universidade Católica do Rio de Janeiro.

Actuators based on piezoelectric materials have ideal characteristics for applications such as acoustic transmission and micromanipulation. However, the inherent nonlinearities of those actuators, such as hysteresis and creep, greatly increase the challenge to control such devices. Furthermore, the increasing need for more precise and faster actuators, allied with frequent changes in the environmental and operational conditions, further worsens the problem. Analytical models are application-specific, meaning that they are not easily and efficiently scalable to all systems. Also, with increased complexity, the understating of underlying phenomena is not fully documented, making it difficult to develop such models. This work investigates those challenges from the perspective of the system identification methodology and data-driven models for piezoelectric actuators. The black-box approach is tested with experimental data acquired in a laboratory setting for micromanipulator and acoustic transmission case studies. In some datasets, general-purpose signals were employed as the excitation input of the system to accelerate the data acquisition of the whole system dynamic and estimation process. Additionally, some models were validated on a separate dataset. In both cases, preprocessing was employed to optimize the amount of data. The tested models include the AutoRegressive Moving Average with eXogenous inputs (ARMAX), Nonlinear AutoRegressive with eXogenous inputs (NARX) with an artificial neural network structure, and Nonlinear AutoRegressive Moving Average with eXogenous inputs (NARMAX). The results show a good ability to predict the nonlinearities of the micromanipulator and, therefore, the hysteresis at different input frequencies. The acoustic transmission system was successfully modeled. Although the results show that there is still room for improvements, it provides insights into possible optimizations for the setup as the models here devised are useful for short prediction windows.

Keywords

Artificial Neural Networks; Black box modeling; Identification and control methods; Piezoelectric Actuators; Nonlinear system identification.

Resumo

Barbosa, Matheus Patrick Soares; Ayala, Helon Vicente Hultmann. **Identificação Não Linear Caixa-Preta de Sistemas Piezoelétricos**. Rio de Janeiro, 2021. 84p. Dissertação de Mestrado – Departamento de Engenharia Mecânica, Pontifícia Universidade Católica do Rio de Janeiro.

Atuadores baseados em materiais piezelétricos apresentam características ideais para aplicações como transmissão acústica e micromanipulação. No entanto, não-linearidades inerentes a estes atuadores, como histerese e fluência, aumentam o desafio de controla-los. Além disso, a crescente necessidade de atuadores mais precisos e rápidos aliada a frequentes mudanças nas condições ambientais e operacionais agravam ainda mais o problema. Modelagens analíticas são específicas ao sistema ao qual foram feitas, o que significa que elas não são facilmente escalonáveis e eficientes para todos os tipos de sistemas. Adicionalmente, com o aumento da complexidade, os fenômenos que regem a física do sistema não são totalmente conhecidos, tornando difícil o desenvolvimento destes modelos. Este trabalho investiga esses desafios do ponto de vista da metodologia de identificação de sistemas e modelos baseados em dados para atuadores piezelétricos. A abordagem de modelagem caixa preta foi testada com dados experimentais adquiridos em um ambiente de laboratório para os estudos de caso de micromanipulação e transmissão acústica. Sinais de uso geral foram empregados como entrada de excitação do sistema de modo a acelerar a aquisição e estimação dos parâmetros. Parte dos modelos desenvolvidos foram validados com um conjunto de dados separado. Em ambos os casos foi necessário pré-processamento para otimização da quantidade de dados. Os modelos testados incluem a Média Móvel AutoRegressiva com entradas eXógenas (ARMAX), AutoRegressiva Não Linear com entradas eXógenas (NARX) com uma estrutura de rede neural artificial e Média Móvel AutoRegressiva Não Linear com entradas eXógenas (NARMAX). Os resultados mostram uma boa capacidade de prever as não-linearidades do micro manipulador e, portanto, a histerese em diferentes frequências de entrada. O sistema de transmissão acústica foi modelado com sucesso. Embora os resultados mostrem que ainda há espaço para melhorias, eles fornecem informações importantes sobre possíveis otimizações para o sistema uma vez que os modelos apresentados são uteis para janelas de predição curtas.

Palavras-chave

Atuadores piezoelétricos; Identificação de sistema não lineares; Métodos de identificação e controle; Micromanipuladores piezoelétricos; Modelagem Caixa Preta.

Table of Contents

List of Figures

List of Tables

List of Abreviations

ACF – Activation function

ANN – Artificial Neural Network

ARMAX – Auto-Regressive Moving Average with Exogenous Input

DOF – Degree of freedom

ELS – Extended least squares

ERR – Error reduction ratio

FRS – Free Run Simulation

MSE – Mean Square Error

NARX – Nonlinear Auto-Regressive with Exogenous Inputs

NARMAX – Nonlinear Auto-Regressive Moving-Average with Exogenous Inputs

OLS – Orthogonal Least Squares

OSA – One Step Ahead

PEA – Piezoelectric actuators

PEM – Prediction error method

ReLU – Rectified linear unit

Rx – Receiver

SI – System Identification

SNR – Signal-to-noise ratio

Tanh – Hyperbolic tangent function

Tx – Transmitter

VNA – Vector Network Analyzer

List of Symbols

A – Amplitude

$G(q)$ – Transfer function from input to output

g_i – Constant coefficient orthogonal to the dataset

$H(q)$ – Transfer function from from noise to output

M – Total number of parameters

nrn – Quantity of neurons of each hidden layer

n_e – Model order of the lags for the noise

n_k – Delay or number of input samples that occur before the input affects the output

n_l – Degree of polynomial non-linearity

n_u – Model order of the lags for the input

n_y – Model order of the lags for the output

$p_i(t)$ – Regressors

R^2 – Multiple Correlation Coefficient

$u(t)$ – Input

$y(t)$ – Measured output

$\hat{y}(t)$ – Predicted output

$w_i(t)$ – Constant coefficient orthogonal to the dataset

α – Decay rate

ϵ – Damping or smoothing factor

η – Learning rate

∇f – Derivative of the loss function

$\phi[\cdot]$ – Activation function

ρ_n – Tolerance of the noise parameters for the error reduction ratio

ρ_p – Tolerance of the parameters for the error reduction ratio

θ – Model parameter, analogous to weight in Artificial Neural Networks

υ_t – Average of gradients

$\xi(t)$ – Residual

El Psy Kongroo

Okabe Rintarō, *Steins;Gate*.

1
Introduction

The piezoelectric effect is an electromechanical property of certain smart materials that produce measurable amounts of electric charge proportional to the mechanical strain applied to the material and vice-versa [1, 2]. This effect is useful in a wide range of devices such as oscillators, resonators, actuators, transducers. In particular, the piezoelectric effect enabled the creation of portable actuators that are widely available commercially. They manage small displacements, in the range of $10pm$ to $100\mu m$, while maintaining high resolution, frequency, stiffness [3, 4], and containing no moving parts, eliminating backlash and friction [2]. According to surveys [2] and [5], Piezoelectric actuators (PEA) are used in micromanipulators and atomic force microscopes to ultra precision machine tools, revolutionizing research in many fields like biology, chemistry, materials, and physics. They can even be used as sensors to provide feedback for control [6–8].

One of the key challenges of PEA emerges from the piezoelectric element itself. They suffer from high nonlinear static and dynamic behavior dependent on frequency, load, and/or amplitude [2]. Also, creep and other thermal effects lead to hysteresis of the PEA and subsequent loss of accuracy [9]. Therefore, any application that requires a high degree of precision, like micropositioning and acoustic transmission, requires that the PEA undergoes some form of control.

The control and automation discipline seeks, in essence, to develop continuous or discrete dynamic systems that behave in a predictable and optimized manner, given the operational conditions to which they are submitted. As such, modeling a system is at the heart of control theory. As modern controllers are designed based on the system to be controlled, modeling and simulation are essential. Several analytical models that take nonlinearities into account to a certain degree, are available in the literature, such as: the Preisach model, Duhem model, Prandtl-Ishlinskii model, and Maxwell model [2, 3, 10–12].

While those models have good modeling capabilities, due to the complex behaviors that are not always fully understood, they require extensive prior knowledge of the system. Therefore limiting the available modeling approaches and their precision due to the knowledge gap between the user and the system.

Moreover, several experiments are needed to determine the application-specific physical parameters and weight functions, often not possible due to equipment availability and/or time constraints. This complexity increases the computation time needed to perform the modeling and further narrows down their potential application uses [11, 13].

In those cases, the application and development of control models are not straightforward or simple. Alternative approaches like the System Identification (SI) methodology allows for easier development with little knowledge of the underlying physical phenomenon or the need for several experiments. SI is a field within automation control that encompasses the creation of dynamic models for the purposes of design, analysis, monitoring, and control of physical systems based on measured data [14]. A good experiment design is needed to allow the data acquisition of finite input-output data with as few interference's as possible. It must be noted that the system is modeled as a whole and, as pointed by [15], this eliminates assumptions that others modeling approaches, such as the analytical models previously cited, sometimes take. Such assumption, like a perfect bonding between the PEA and the structure, creates an inconsistency between the model and the real system, decreasing its accuracy [16]. Furthermore, as the SI approach utilizes experimental input-output data acquired directly from the system, it captures any dynamic behavior even if its unknown by the user. Therefore the model faithfully represents the system [16].

1.1 Literature Review

A system can be described as an object that through the interaction of different inputs, even unwanted external disturbances or noise, produces an observable signal, also called an output [17], as shown in Figure 1.1. One of the properties of a system is its state, which summarizes the effects of the past inputs and noise. Those kinds of systems are called open loop systems and are suitable for the SI methodology [18, 19].

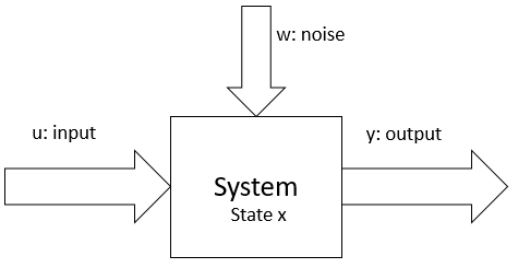

Figure 1.1: Schematic of an open loop system. Adapted from [18].

With this in mind, the SI methodology has been applied successfully to a wide range of systems outside the realm of engineering, such as biology in general [20–24] and water resource management and monitoring [25, 26], to cite a few. The available models in SI methodology can be categorized based on the required knowledge of the underlying physics (white-box, gray-box, or black-box), based on the presence of error (deterministic or stochastic), or its structure (Parametric or Non-Parametric) [14, 27].

Generic PEA modeling using SI methodology studies such as [13, 28–30] show the effectiveness of the approach. The authors in [13] accurately describe static and dynamic hysteresis with generic use of PEA. Employing a nonlinear moving average model with exogenous inputs and Nonlinear Auto-Regressive Moving-Average with Exogenous Inputs (NARMAX) for the static and dynamic hysteresis modeling respectively. In [28] and [29] the authors used Artificial Neural Networks (ANN) to model the hysteric behavior of PEA. The second experimentally compared the effectiveness of the approach to other techniques such as commercial controllers and a Duhem-based model. In [30] the authors proposed the use of a hybrid approach, where the use of ANN, in addition to the Preisach model, improved the capabilities of the semiempirical model that lacked the modeling of frequency-dependent behavior.

Still, some examples of limitations of the aforementioned works are the lack of model validation, lack of guidelines/assumptions taken in the signal design, and the test of the piezoelectric element under no load. This leads to the belief that the results could lack meaningful significance in real-world specific applications. Otherwise, generic PEA modeling studies provide useful insights into the overall SI procedure and a guideline on what could work. Nevertheless, several studies are found that aim to simulate real-world specific applications of PEA [16, 31–33].

In Vibration Control, the authors in [16] and [31] used the SI methodology to successfully create an equivalent linear model based on a Finite Element Analysis of PEA. Then validated it through a specially made workbench to acquire the experimental data.

In Nano and Micro Manipulators PEA are found in biomaterial and cell manipulation, nanomanufacturing and machining, high-resolution probe microscopy, and so on [34–38]. They take advantage of some of the PEA benefits, such as fast response and high stiffness. However, in some applications, their low displacement can limit their use directly. In those cases, mechanical amplification can be leveraged to increase the displacement to useful levels at the cost of size, speed, or even reliability. This can be achieved by altering the PEA design and, according to [39], they are categorized in: i) externally

leveraged; ii) internally leveraged, or iii) frequency leveraged.

The simplest is the stack, where several piezoelectric elements are linearly bounded together creating an overall bigger displacement. Another type is the bender, which is similar to a cantilever and has the advantage of quadratic amplification as a function of its length. By applying an electric potential, the piezoelectric element bend and this bending is exploited to push and manipulate small objects [40]. Both stack and bender are classified as internally leverage. As the PEA design influences its performance, it is expected that it also alters its response to the input and consequently the system dynamics, further narrowing down the modeling to the specific system [39].

In [32], the authors modeled a 1-Degree of Freedom (DOF) micromanipulator and in [33], a 2-DOF micromanipulator. Both proved the viability of utilizing a shallow ANN based on the Nonlinear Auto Regressive with Exogenous Inputs (NARX) model with increasing complexity to predict and model the PEA hysteresis at high frequencies. However, a limitation of both works is the lack of verification of adherence of the model through specific frequency bands.

Also, ANNs have been long used for SI [41]. Architectures such as Radial basis functions [42] and multilayer perceptrons [43] are valuable tools for nonlinear modeling. However, deep learning has not been extensively applied in SI in order to solve complex dynamic systems modeling tasks, despite its impressive improvements mainly in the field of image processing [44]. It consists of constructing deep neural networks, with many hidden layers and neurons, forming models with thousands, and even millions, of parameters to set. Thus, enabling several layers of representation, aiming at increasing the capability of the models in solving complex systems.

In [45] the authors used a Boltzmann machine trained with random weights and validated the model using data from standard SI benchmarks such as: gas furnace data [46], simulated nonlinear system [47] and the Wiener-Hammerstein case study [48]. In [49], the authors employed partial least squares regression to estimate a deep neural model and evaluated the methodology with a simulated nonlinear chaotic system, and by using acquired data predicted the amount of phosphorus in the wastewater treatment system. Thus, there is an opportunity for improvement in micromanipulator modeling by means of deep neural networks.

For applications of acoustic transmission, the PEA creates a mechanical wave that requires a medium to propagate. Due to its nature, it can be applied to scenarios where other means of communication are not efficient or feasible [50]. For example, wired communications through pressure vessels introduce a

puncture on the walls and another possible point of failure. Another case is the presence of metal enclosures where the strong Faraday cage effect reduces the efficiency, or even makes it impossible to use certain techniques, such as inductive coupling, capacitive coupling, and magnetic resonance coupling of electromagnetic waves [51, 52]. In those cases, a PEA can be bonded to the interior and exterior walls creating an acoustic channel, enabling data transmission [53], energy [54,55], or both simultaneously [52,56]. As one might expect, the acoustic channel properties have a great impact on transmission efficiency. This is further exacerbated by the use of multiple layers of different materials, energy losses due to unwanted reflections and vibrations, and the existence of discontinuities in the transmission medium, among other factors [50, 57, 58].

Although several studies for generic PEA modeling and piezoelectric based micromanipulator modeling are available in the literature, for the case of acoustic transmission systems, they are scarce. Making clear that the available methods, mainly the general multilayered case, are still open for debate and improvement. Nevertheless, related transmission applications, such as magnetic coupling [59, 60], are useful as a starting point.

1.2 Motivation and Objectives

Through the literature review, it is clear why the use of PEA has become increasingly intense in the last decade. The advantages that these actuators bring over conventional ones are numerous, such as their high resolution, frequency, and stiffness. However, with the increasing need for process agility, at higher load levels, these actuators suffer from non-linear effects, making proper control a challenge. The development of analytical models has been proved to be effective but they depend on complex solutions, demanding, in addition to processing power, high knowledge of the system in which they will be used. Thus, they are application-specific and require several experiments.

The use of the SI methodology, especially black-box models, on piezoelectric based systems allows the creation of models more quickly and with sufficient precision for application in real scenarios. However, in spite of several quality works that apply the SI methodology successfully to PEA, to the best of our knowledge, there is a lack of proper development of a model for the general multilayered case of acoustic transmission. Additionally, deep learning needs more research time for dynamic systems.

Therefore, the main goals of the present work are the following:

– Explore how deep learning models can describe hysteresis originated from

the nonlinearities in piezoelectric based micromanipulation;

– Investigate, through the use of the SI methodology, which models are more appropriated to describe a multilayered piezoelectric based acoustic transmission system of data and/or energy.

To accomplish these, two case studies are devised based on real-world applications, namely: piezoelectric micromanipulator and piezoacoustic transmission. Suitable test benches, to enable reliable experimental data acquisition, are also developed. The details of each case study and its respective setup are devised in Chapter 3.

As the SI black-box models have potential in real-world applications, a side objective is to show the importance of multisine signals for hysteretic systems, as pointed by [61].

1.3 Original Contributions

All three contributions, ordered by submission date, are properly referenced below:

1. SOARES BARBOSA, M. P.; RAKOTONDRABE, M. ; HULTMANN AYALA, H. V.; **Deep learning applied to data-driven dynamic characterization of hysteretic piezoelectric micromanipulators**. IFAC-PapersOnLine, 53(2):8559–8564, 2020. 21th IFAC World Congress.

2. SOARES BARBOSA, M. P.; DA COSTA, D. P. ; HULTMANN AYALA, H. V.; **Evaluation of nonlinear system identification to model piezoacoustic transmission**. IFAC-PapersOnLine, 53(2):8802–8807, 2020. 21th IFAC World Congress.

3. SOARES BARBOSA, M. P.; HULTMANN AYALA, H. V.; **Evaluation of Deep Artificial Neural Networks for Data-driven Modeling of Piezoacoustic Transmission**. (Manuscript in Preparation)

Regarding the piezoelectric micromanipulator case study, SI methodology was utilized and the steps to acquire and process the data were devised. Several deep-learning neural network architectures were tested and compared. The training excitation signal was a general-purpose multisine spanning the frequency band of interest. Finally, the best model was decided based on metrics and it was further validated with semi-static individual sinusoidal curves of different frequencies. Therefore, verifying the adherence of the model through the frequency domain. The results indicate the usefulness

and predictive power of deep learning-based models in the field of system identification and, in particular, hysteresis modeling and compensation in micromanipulation applications.

Regarding the piezoacoustic transmission case study, two separated datasets were acquired. Those employed the same test bench but different signals. While the first was more of a survey, employing three AutoRegressive models, including the Auto-Regressive Moving Average with Exogenous Input (ARMAX), NARX, and NARMAX, and used a chirp signal as the estimation. The last was an in-depth analysis and expansion of the NARX approach using a multisine signal as estimation and chirp as validation. The results compare each model tested and provide insights into improvements that can be made.

1.4 Manuscript organization

This work is organized as follows: Chapter 1 aims to introduce and contextualize the specific applications of PEA through the literature. The motivation and objectives are discussed and a brief introduction to the case studies is made.

Part I aims to present the theoretical basis and key concepts in the SI general procedure and details of the case studies. All the necessary steps and methodologies used in data acquisition, preprocessing, and models are devised in Chapter 2, and details of both cases studies are shown in Chapter 3.

In Part II the results of the contributions of the present work are shown.

Conclusions and additional remarks for future works are presented in Part III.

Part I

Methods

2
System Identification methodology

The general procedure for identifying a system based solely on experimental data is shown in Figure 2.1.

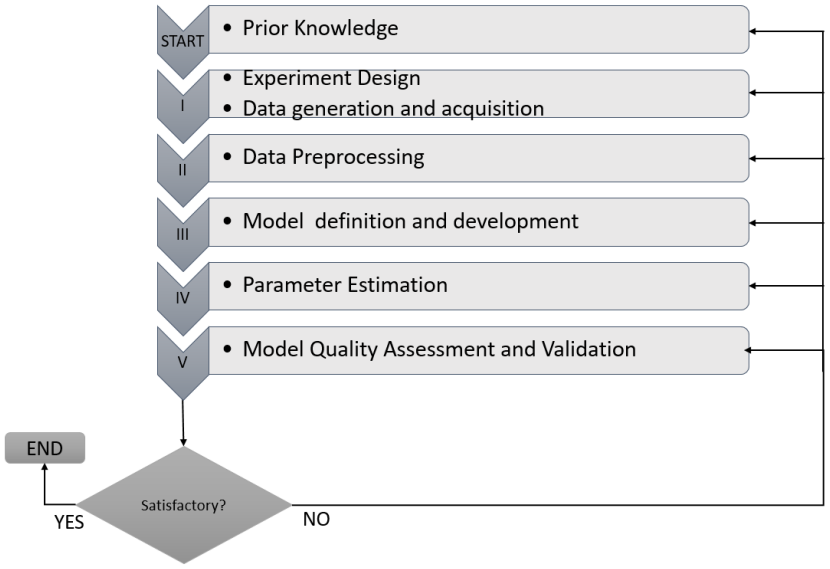

Figure 2.1: System identification procedure, adapted from [62].

This methodology is an iterative process where, although prior knowledge is not entirely required, if combined with a clear objective, it can significantly accelerate the process. Even if a good prior knowledge is available, it can change after several interactions of the procedure, leading to a better understanding of the system and improvements in the overall SI loop [18].

It is generally not possible to create an exact mathematical description based on a finite number of samples. This is influenced by several factors like input type, signal-to-noise ratio (SNR), presence of errors, randomness, to cite a few. Even with perfect conditions, usually it is not desirable to have a 100% precise model due to increasing complexity in real-world applications. Consequently, the SI methodology creates an approximate model for system [14, 27].

2.1 Experiment Design and Data acquisition

Naturally, the first step is to acquire the data and, to alleviates the influence of the aforementioned factors, a solid experiment is needed. Although a simple task at first glance, the accuracy or confidence of the model will be as good as the available data, both in terms of quality and quantity [18]. As such, even the sampling rate must be carefully analyzed, because relevant information can be hidden in the frequency domain and by limiting the sampling rate, this data is lost [14]. It is also important that any source of noise and/or disturbances, that may contaminate the measurements, have a low relative amplitude to the data of interest, which is called sensitivity.

Regarding the sampling rate, it should be fast enough to extract all data available in the system. The Nyquist-Shannon Theorem [63] states that the minimum sampling rate needed for a continuous signal to be completed recovered is $2f_c$, where f_c is the highest frequency in the signal band. However, as pointed by [27], over-sampling provides little benefit as it increases the necessary lags to correctly estimate the model parameters. Often $5f_c/2$ is sufficient, but spectral analysis and correlations benefit from a higher sampling rate, in the order of $10f_c$. The overall recommendation is to use the fastest sample rate possible, which means oversampling the experiment, as one can decimate it later, instead of performing a new experiment due to slow sample rate or trying to interpolate the data and introduce errors and noise [27].

Furthermore, other sources of influence, like the probing equipment itself, must be analyzed as it alters the characteristics of the system under study and contaminates the data.

2.2 Excitation Signal Design

The choice of the excitation signal is particularly critical. It affects the overall model estimation and must be taken such that the acquired data contains as much information about the dynamic properties of the system in question as possible. General-purpose signals can stimulate the system with an almost flat power spectrum in user-defined broadband. As such, it can reduce the measurement time as it captures the whole dynamic in the band of interest when compared to a signal that excites the system frequency by frequency. Additionally, those signals can be parameterized according to a range of amplitude and frequency band of interest. Therefore the signal statistics can be tuned to an application-specific system and the optimization/maximization

of the sensitivity can be achieved [14, 18, 64]. Examples of such signals are multisine and chirp [65].

A multisine signal is a sum of several sinusoidals of different frequencies, which are predefined. The multisine signal is defined by:

$$u(t) = \sum_{k=1}^{n_f} A\cos[2\pi f_k t + \phi_k] \tag{2-1}$$

where f_k and ϕ_k are, respectively, the frequency and phase of each sinusoidal component and A is the amplitude.

The spectrum is not continuous as each f_k may be determined equally spaced between a minimum and maximum value of interest with n_f components. It is computationally easier to define those components in the frequency domain and then use the inverse Fourier transform to get the signal in the time domain [65, 66].

A useful guideline is to keep the sines out of phase to keep the crest factor low [14]. So the phase ϕ_k can randomly set in the range $[0, 2\pi]$ for each component, becoming a Random Phase Multisine. By using $\phi_k = -k(k-1)\pi/n_f$, it is called the Schroeder Multisine [67].

The number of components n_f should be large enough so that the frequency resolution is sufficient for the identification, being dependent on the system and model order [17].

This signal exclusively excites the band of interest and provides good estimation at the frequency components defined, providing great flexibility by allowing dedicated selection of amplitude and frequencies, making it possible to detect and quantify the presence of nonlinear distortions [65].

Another broadband signal is the chirp, also called swept sine or periodic chirp. It is a type of signal where the frequency changes with time and is repeated in a way to create a periodic signal [17,65]. The simplest form changes the frequency linearly with period T_0 and is calculated by:

$$u(t) = A\cos((at+b)t) \qquad 0 \leq t < T_0 \tag{2-2}$$

Where A is the amplitude, $a = \pi(k_2 - k_1)(f_0)^2$ and $b = 2\pi k_1 f_0$, $f_0 = 1/T_0$, $k_2 > k_1 \in \mathbb{N}$ and $k_1 f_0$, $k_2 f_0$ are the lowest and highest frequency respectively. Contrary to the multisine, the spectrum is not as flat. Consequently this introduces frequency components with lower SNR and, due to the sliding frequency, spectral lines appearance outside the band of interest. Nevertheless, it should not be disregarded as a inferior signal as it injects more power into the system than the multisine, as pointed by [65].

Different from the chirp, the pure sinusoidal is not a broadband signal and as such, the acquisition process is usually slower compared to it. The stimulus of several frequencies is called step sine, as the system needs to be excited for a specific amount of time. A waiting time should be included to allow transients to disappear before the next step and it is proportional to the damping present on the system. When few frequencies are needed to model a system and the SNR is poor, the pure sinusoidal can prove to be a faster method, compared to a broadband signal, as it concentrates the power in one specific frequency, overcoming the poor SNR. When the number of frequencies to excite is large, this approach loses its advantage [65]. It is defined by:

$$u(t) = A\cos[f_0 t + k_0] \tag{2-3}$$

where k_0 is the initial phase in the range $[0, 2\pi]$, f_0 is the desired frequency and A is the amplitude. Nevertheless, they are useful to evaluate the model adherence and performance to each specific frequency, enabling the creation of hysteresis loops.

2.3 Signal Preprocessing

In the majority of cases, even with a careful experiment and signal design, the data can still have some degree of inconsistency. Therefore, an additional step to preprocess the data, prior to the choice of the model, is necessary. The raw data can be contaminated by outliers, drifts, shifts, high or low-frequency disturbances, and even missing points. However, even in the absence of any kind of quality problems, or if the user decides to pass this burden to the model as an additional noise, the data can be further optimized. By reducing the number of points its possible to alleviate the computational cost and greatly reduce the time necessary in the next steps. One must exercise caution to preserve the characteristics of the signals in both time and frequency domains, in the region of interest [14, 17].

A good data inspection is often a key step as it can reveal a lot of insights regarding not only the presence of the aforementioned peculiarities in the data, but enabling to qualitatively analyze and assert its quality, like the SNR. A visual inspection in a transformed domain, besides the time domain, such as the frequency domain, allows for a deeper analysis and can lead to further insights and valuable information [14, 17].

Regarding outliers and missing data, two of the most common problems in the analysis, they can severely diminish the accuracy of the model. The

first is an observation, or a group of them, that deviates severally from the neighbors, influencing the signal properties such as mean, standard deviation co-variance, spectral density, to cite a few. The second breaks the continuity of the data and traditional techniques, based on regularly spaced observations, do not work [14].

One way to deal with those is to cut out the bad segments, then merge the good ones. This is applicable also when a separate number of experiments have been performed due to equipment availability. However, for datasets with multiples inputs and outputs, it might be difficult to find segments where all variables are assumed good. In those cases, it is usually recommended to treat outliers as missing data [17].

Beyond outliers and missing data, trends, drifts, offsets, and other non-stationary behaviors must be also removed, especially if the methods assume that the statistical properties of the data remain invariant with time. Unknown time delays can be accommodated by the model during the identification, but obvious shifts are easier to be removed, since they pose a problem when using mean, correlation or spectral analysis, and during the parameter estimation. Drifts and trends are time-varying originated from the inherent non-stationary process or disturbances in the system. They can be seasonal or not [14, 17, 27]. One must note that some methods to remove those, such as differentiation or noise model with integration, can increase the noise floor and, in the case of offsets, push the model to fit into a high-frequency region, which can be unsuitable for some applications [17, 27].

Generally, removing noise is not recommended because it is impossible to differentiate it from valuable information. In general, a careful experiment design and reliable data acquisition can alleviate the aforementioned problems and noise, saving time on the overall loop. One must practice moderation in the preprocess to not alter profoundly the dynamics of the system present in the input-output data acquired [14, 27].

Lastly, assuming that the data has been correctly sampled, signal pre-processing can help to optimize the amount of data and reduce the number of samples. This is important to reduce the computational burden and can be achieved by the simple use of decimation or other filters, like Moving Average. Some estimation methods, like the Orthogonal Least Squares (OLS) algorithm, can be applied directly to all points up to five hundred samples. Above five hundred and up to two thousand samples, the data can be divided into over-lapping segments and the OLS applied to each of them, increasing the overall speed compared to the use of all points simultaneously [27].

2.4 Model types

A model can be described as a mathematical description that can be categorized according to the approach used in the development: i) theoretical based on fundamental laws (first-principles or white-box), ii) empirical based on observations (experimental or black-box) [14, 27]. Figure 2.2 shows a comparison between the types of models regarding the number of experiments and the knowledge of the system required.

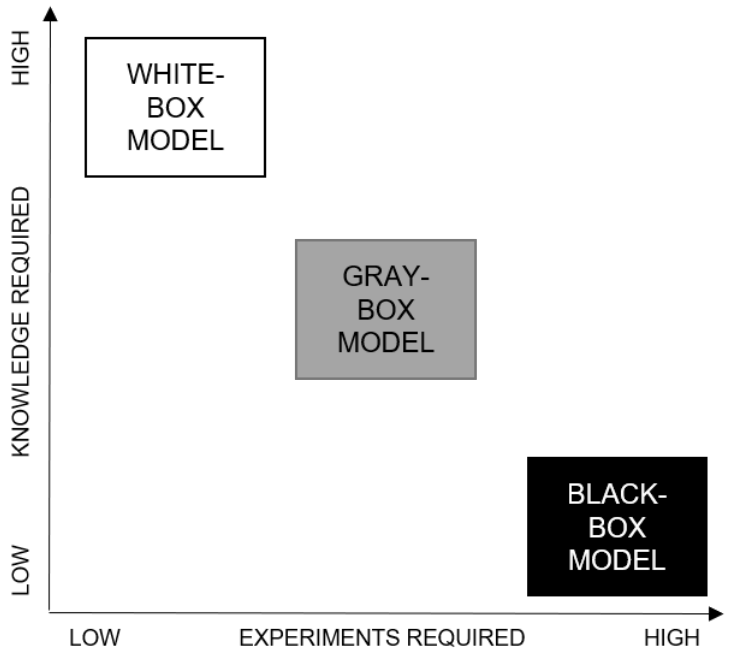

Figure 2.2: Model types comparison regarding the number of experiments and the system knowledge required.

The first approach requires that a system is broken in its parts and, assuming a good understanding of the underlying physics of each part is available, the model description is built by applying natural laws. This brings transparency, as one can easily read the model as it has physical meaning. On the other hand, the drawback is that the required knowledge is not always available, this is further exacerbated by increasing system complexity, demanding more time and resources to create a problem-dependent theoretical model [14, 27].

The empirical approach overcomes the aforementioned challenges and is generally applicable to all systems. By using experiments to acquire sufficient data, it is possible to extract the dynamics of the system buried in the data and figure out what the underlying model should be to achieve the relationship between the inputs and outputs. The downside is that, compared to the

first-principles or white-box models, the black-box model lacks transparency (opaque) and physical meaning. Moreover, as it utilizes a finite number of samples, the generalization capabilities of the data-driven approach is worse, being capable of good extrapolation in the limited operation envelope that the data contains [14, 27]. However it has flexibility as it can be applied to linear and nonlinear systems [68].

By combining the theoretical properties of the white-box with data, the gray box is an in-between type of model that combines the advantages and mitigates the weakness of the pure white-box and black-box models [69]. The possibility to include prior knowledge directly in the model yields fewer and more tangible parameters than the black-box. Furthermore, in contrast to the white-box approach, it can better deal with noise and randomness, leading to improved results [70].

2.5 Model Choice

There is not a definitive answer in the literature for which architecture is the best for an application. Experimentation can be time-consuming, so one may take advantage of similar works to narrow down the alternatives.

If none are available, generally, a piece of good advice is to try simple models first. Some thought in how the relationship between inputs and outputs can give a head start in the model selection. Additionally, intuition and ingenuity can be leveraged here [17].

As stated in the previous section, three types are available based on the approach and amount of knowledge necessary of the underlying physical phenomena. This work focuses solely on the empirical approach or black-box models.

The Auto-Regressive Moving Average with Exogenous Input (ARMAX) is popular in procedures for control design. It is an extension of the Auto-Regressive with Exogenous Inputs family of models and includes a moving average component in the noise model [18]. It can be described as:

$$\begin{aligned} y(t) + a_1 y(t-1) + \cdots + a_{n_y} y(t-n_y) = \\ b_1 u(t-n_k) + \ldots + b_{n_u} y(t-n_k-n_u+1) + \\ c_1 e(t-1) + \ldots + c_{n_c} e(t-n_e) + e(t) \end{aligned} \tag{2-4}$$

where y, u, and e are respectively output, input, and the noise signals and n_u, n_y and n_e are their respective orders. The term n_k is the delay, meaning the number of input samples that occur before the input affects the output. In

this work $n_k = 0$.

The compact form of the ARMAX model can be described as:

$$A(q)y(t) = B(q)u(t - n_k) + C(q)e(t) \tag{2-5}$$

where $A(q)$, $B(q)$, and $C(q)$ are the polynomials to be estimated.

The NARMAX is a parsimonious nonlinear model that, similarly to the ARMAX, includes noise terms to accommodate disturbances in the system. Moreover, it is based on expansion of past inputs and outputs, but it includes nonlinear terms. The term NARMAX can also be found on the literature as a philosophy of nonlinear system identification [27,71]. The general definition of the model is:

$$\begin{aligned} y(t) = F[&u(t-1), \ldots, u(t-n_u), \\ &y(t-1), \ldots, y(t-n_y), \\ &e(t-1), \ldots, e(t-n_e)] + e(t) \end{aligned} \tag{2-6}$$

where y, u, and e are the system output, input, and noise signals respectively, $F[.]$ is a nonlinear function and n_u, n_y and n_e are the order of the lags for the input, output and noise respectively. The objective is to find the function $F[.]$ that correct simulates the system [27]. The case of the polynomial NARMAX, which is the most commonly used form, the compact definition is:

$$\begin{aligned} y(t) = \theta_0 + \sum_{i_i=1}^{n} \theta_{i_1}(x_{i_1}(t)) + \sum_{i_1=1}^{n}\sum_{i_2=i_1}^{n} \theta_{i_1 i_2}(x_{i_1}(t)x_{i_2}(t)) + \ldots \\ + \sum_{i_1=1}^{n} \cdots \sum_{i_{n_l}=i_{n_l-1}}^{n} \theta_{i_1 i_2 \ldots i_{n_l}} \left(x_{i_1}(t)\, x_{i_2}(t)\, \ldots\, x_{i_{n_l}}(t)\right) + e(t) \end{aligned} \tag{2-7}$$

where $\theta_{i_1 i_2 \ldots i_l}$ are model parameters to be estimated, with $n = n_u + n_y + n_e$. The first sum concerns linear terms, the second sum, the nonlinear terms of second order, and so on until the last sum that concerns terms of order n_l, which indicates the degree of polynomial non-linearity. $x_{i_1 i_2 \ldots i_l}$ can assume the form of input, output, or noise, such as [27]:

$$x_i(t) = \begin{cases} y(t-i) & 1 \leq i \leq n_y \\ u\left(t - (i - n_y)\right) & n_y + 1 \leq i \leq n_y + n_u \\ e\left(t - (i - n_y - n_u)\right) & n_y + n_u + 1 \leq i \leq n_y + n_u + n_e \end{cases} \tag{2-8}$$

with n_u, n_y and n_e are the order of the lags for the input, output and residual respectively.

The NARX model, on the other hand, is a especial case of the NARMAX that does not include noise-dependent terms [27]. The definition in equation

2-7 becomes:

$$\begin{aligned} y(t) = F[&y(t-1), y(t-2), \ldots, y(t-n_y), \\ &u(t-1), u(t-2), \ldots, u(t-n_u)] + e(t); \end{aligned} \tag{2-9}$$

Similarly to equation 2-7, n_y and n_u are the maximum lags (or orders of the model) at the output and the input, $e(t)$ is an independent noise sequence and $F[.]$ is a nonlinear function. In the case of the NARX, some examples of functions are the ANN, wavelet network, or sigmoid network.

The ANN have been extensively used for SI [41]. Several architectures exist, but Radial Base Function [42] and multilayer perceptrons [43] are between the most valuable tools for the identification of black box systems. Nevertheless, deep learning has received considerable attention recently, due to impressive improvements mainly in the field of image processing [44]. It consists of many hidden layers and modular units, which form models with millions of free parameters to set [72, 73]. Following the notation in [72], deep neural models for regression may be described as:

$$\hat{r} = \phi \left[\sum_k \theta_{ok} \phi \left[\sum_j \theta_{kj} \phi \left[\ldots \phi \left[\sum_i \theta_{li} x_i \right] \right] \right] \right] \tag{2-10}$$

where θ_{ok} is the synaptic weight from $k-th$ to $o-th$ layer and $\phi[\cdot]$ is the neuron activation function (ACF), which can be set, for example, as a sigmoid, hyperbolic tangent (tanh) or rectified linear unit (ReLU), described respectively by:

$$\phi(z) = 1/(1+e^{-z}) \tag{2-11}$$

$$\phi(z) = tanh(z) \tag{2-12}$$

$$\phi(z) = \max(0, z) \tag{2-13}$$

The use of ReLU as an ACF is popular and recommended for most feed-forward structures because: (i) Beyond the fact that ReLU have half of the domain as zeros, they behave very closely to a linear ACF, being called a piecewise linear function. As such, they preserve the characteristics of linear models that are far easier to optimize and overcome some of the problems of sigmoidal and tanh regarding the gradient vanishing effect due to nonlinearities [74]. (ii) Besides the not differentiable point at $z = 0$, they have a large and constant derivative through the nonzero region (active neuron). Also, the second derivative is

always zero. This simplifies the optimization when compared to other ACF that introduces second-order terms [74, 75].

One drawback of ReLu arises because of its non-linearity present at the origin. As such, they cannot be used in situations where the activation is equal to zero and gradient-based training methods are used. In practice, this method still performs because, usually, it is not expected that an ANN reaches the exact local minimum of the loss function [74].

As Equation 2-10 can be thought of as a collection of nonlinear static activation units, ϕ, it lacks any dynamics due to missing lagged inputs and outputs. For applications that do not require dynamic behavior, such as pattern recognition, this is not an obstacle. However, it poses a problem for prediction applications such as time-series [27]. To circumvent it, a feedback loop must be used, creating a recurrent neural network model or by explicitly supplying the network with lagged inputs and outputs.

In the later, the inputs of the model are defined as the inputs in Equation 2-9, namely the lagged inputs and outputs of the NARX model, differently from the recurrent approach. So, as pointed by [72], the input vector is composed of:

- The current and past input values originated from outside the network, $u(p-2), \ldots, u$
- Delayed values of the output, on which future values are regressed from the network

In order to create the model we need to build the regression matrix and the target values, described respectively below:

$$\Phi = \begin{bmatrix} y(p-1) & \ldots & y(p-n_y) & u(p-1) & \ldots & u(p-n_u) \\ y(p) & \ldots & y(p+1-n_y) & u(p) & \ldots & u(p+1-n_u) \\ y(p+1) & \ldots & y(p+2-n_y) & u(p+1) & \ldots & u(p+2-n_u) \\ \ldots & \ldots & \ldots & \ldots & \ldots & \ldots \\ y(N-2) & \ldots & y(N-1-n_y) & u(N-2) & \ldots & u(N-1-n_u) \\ y(N-1) & \ldots & y(N-n_y) & u(N-1) & \ldots & u(N-n_u) \end{bmatrix} \tag{2-14}$$

$$Y = \begin{bmatrix} y(p) \\ y(p+1) \\ \vdots \\ y(N) \end{bmatrix} \tag{2-15}$$

where $p = 1 + max(n_y, n_u)$, u is the input and y is the measured output. They are fed as training examples for the deep neural network during estimation.

2.6 Estimation

The two main categories of estimation are parameter and signal estimation. In this work, estimation assumes the role of parameter estimation, also known as training when referring to ANN models. It refers to the determination of unknown parameters (or weights), of the mathematical abstraction (or model), that best relate to the underlying system, based on known information. The information can be presented in several forms such as time-series data, images, and/or initial conditions, to cite a few. The expression, algorithm, or device that computes and performs the estimation is called an estimator. Those can be compared to a filter, as it selective chooses the parameters from the known information or given observations [14].

The preferred characteristic of a good estimator is that it defines the parameters of the model as such that it (i) defaults to the simplest possible model; (ii) is as transparent as possible; (iii) provides the closest possible estimate to the "true value" of the parameters [14, 27].

Whether or not a true value exists, the estimator may not produce it due to the existence of (i) uncertainties in the data, (ii) modeling errors, or (iii) the impossibility to reach the global minimum. Nevertheless, it is important to have a metric of how good obtained result is and have confidence intervals where the true values are expected to be contained. Therefore the use of an estimator is accompanied by tests to assess its performance. According to. [14] there are essentially six measurements that can be performed on an estimator:

1. **Bias:** Statistical average of all possible results of an estimator to assert the accuracy;
2. **Variance:** Statistical spread of all possible results around their average to assert the repeatability;
3. **Mean squared error:** Also knows as MSE, it is similar to the variance but the reference point is the true value instead of the average;
4. **Consistency:** Useful to check if a larger sample size can improve the result by measuring the behavior of a large sample of the MSE;
5. **Efficiency:** Useful to compare two estimators;
6. **Sufficiency:** Determines if the estimator is suitable for a given problem by analyzing if it left the dynamic of the system in the data.

Even though several estimators exist, the foundation methods are: Methods of moments, Least-squares, Maximum likelihood estimation, and Bayes [14].

Despite the fact that the ARMAX is in the same family of the ARX model, the estimation procedure is more complex. To correctly estimate it, an iterative method is needed. Such method includes the recursive prediction error method (PEM), generalized least squares, instrumental variables, or extended least squares (ELS) [27].

PEM methods minimize the cost function trough numerical optimization. The principle is to determine θ that minimizes the residuals in the following equation:

$$e(t,\theta) = y(t) - \hat{y}(t|t-1,\theta) \tag{2-16}$$

where $\hat{y}(t|t-1,\theta)$ is the prediction performed using measured data up to $t-1$.

Similar to the ARMAX, the NARMAX also requires an iterative method. The definition in Equations 2-6 and 2-7 includes all possible candidates of terms, calculated by $M = (n+l)!/[n!l!]$ where $n = n_u + n_y + n_e$. As such, to achieve its parsimonious characteristics, an algorithm is needed to select the most relevant terms by calculating its contribution to the model output.

Once the structure has been defined, the parameters and noise series can be estimated. The OLS associated with error reduction ratio (ERR) is a solution that meets the desired characteristic of an estimator [27]. Given a generic representation of a linear-in-the-parameter model:

$$\sum_{i-1}^{M} p_i(t)\theta_i(t) + e(t) \tag{2-17}$$

where θ and M are the parameters to be estimated and the total number of parameters, respectively, $p_i(t)$ are the regressors and $e(t)$ is the noise. The OLS transform the regressors in equation 2-17 into a orthogonal vector, then equation 2-17 becomes an auxiliary model [27]:

$$\sum_{i=1}^{M} w_i(t)g_i + e(t) \tag{2-18}$$

where g_i are constant coefficients and $w_i(t)$ is orthogonal to the dataset constructed by [76]:

$$\sum_{i=1}^{N} w_i(t)w_j(t) = 0 \tag{2-19}$$

with $i \neq j$. Once each parameter is estimated, the ERR calculates the

contribution of each term and represents, through a percentage, the reduction with respect to the output MSE [76]. The ERR introduced by the i-th term can be described as:

$$ERR_i = \frac{{g_i}^2 {w_i}^2(t)}{y^2(t)} \, i = 1, 2, \ldots, M \tag{2-20}$$

where y and w_i are both the expected values for the output and the orthogonal dataset. A higher value of ERR indicates a higher contribution of the term to the reduction of the model error. Then the term is included if [76]:

$$1 - \sum_{i-1}^{M} ERR_i < \rho_p \tag{2-21}$$

where ρ_p is the tolerance of the parameters defined by the user. Additionally, the ERR can have a separated threshold to be used for the noise term, ρ_n. By reordering the regressors $p_i(t)$ in Equation 2-17 the ERR criteria can be affected. Therefore, depending of the order that they are written down, it may provide a different outcome [27]. The Forward Regression Orthogonal Least Squares (FROLS), also known as orthogonal forward regression algorithm, aims to avoid it by improving the basic OLS principles to select the most relevant and important terms. As the NARMAX from Equation 2-7 belongs to the following representation of a linear-in-the-parameter model [27]:

$$y(k) = \sum_{m=1}^{M} \theta_m p_m(t) + e(t) \tag{2-22}$$

where θ_m are the model parameters and p_m the model terms defined as:

$$\begin{aligned} p_m(t) =& y\left(t - m_{y,1}\right) \cdots y\left(t - m_{y,my}\right) u\left(t - m_{u,1}\right) \ldots \\ & \cdots u\left(t - m_{u,mu}\right) e\left(t - m_{e,1}\right) \cdots e\left(t - m_{y,ey}\right) \end{aligned} \tag{2-23}$$

with $i = 1, 2 \ldots M$ and $my, mu, me > 0$. The improvement occurs by ordering the terms such that:

$$\begin{aligned} 1 \leq m_{y,1} \leq m_{y,2} \leq \cdots \leq m_{y,my} \leq n_y \\ 1 \leq m_{u,1} \leq m_{u,2} \leq \cdots \leq m_{u,mu} \leq n_u \\ 1 \leq m_{e,1} \leq m_{e,2} \leq \cdots \leq m_{e,me} \leq n_e \end{aligned} \tag{2-24}$$

So, $m_y = 0$ indicates that $p_m(k)$ contains no $y(\cdot)$ terms. $m_u = 0$ indicates that $p_m(k)$ contains no $u(\cdot)$ terms. And $m_e = 0$ indicates that $p_m(k)$ contains no $e(\cdot)$ terms.

Therefore, through iterations of the remaining not selected candidate

terms, a full search is performed to assert if a term passes the ERR test based on the parameters defined by the user until all terms are either selected or disregarded. The limitation of this approach is that it cannot estimate the moving average terms in the NARMAX models [27].

Further optimizations can be achieved by employing the ELS-FROLS strategy, overcoming the limitation of estimation of moving average terms [71]. The basic steps are the following:

1. Parameter definition based on orders n_u, n_y, n_e, and n_l;
2. Selection of terms according to user-defined threshold ρ_p using FROLS;
3. Selection of noise terms according to a user-defined threshold ρ_n;
4. Estimation of the parameters, based on the selected terms, using any least-squares procedure.

Training ANNs requires a different approach due to its stochastic nature. The Root Mean Square Propagation Algorithm (RMSprop), which according to [77] has been proposed by [78], is similar to the gradient descent with momentum. However, it differs when updates the weights as it divides the gradient by a running average of its recent magnitude and it is capable of individualizing the learning rate for all model parameters, providing improvements as the parameter scales may differ across the network thus speeding up convergence [79, 80]. It is defined as:

$$\upsilon_t = \alpha\upsilon_{t-1} + (1-\alpha)(\nabla f_t)^2 \tag{2-25}$$

And the update step is given by:

$$\theta^t = \theta^{t-1} - \eta\frac{\nabla f_t}{\sqrt{\upsilon^t} + \epsilon} \tag{2-26}$$

where ∇f is the derivative of the loss function with respect to the parameter θ to be updated (weight), υ_t is the average of gradients, η is the learning rate, α is the decay rate or the moving average parameter and ϵ is the damping or smoothing factor.

The training algorithm needs a quantity that it should seek to minimize. This is called a loss function, or objective function, and the Mean Squared Error (MSE) was used. It is defined as:

$$MSE\left[x, \theta; p\right] = \frac{1}{N}\sum_{i=1}^{N}\left[y_i - \hat{y}_i\right]^2 \tag{2-27}$$

where N is the total amount of input/output pairs. It computes the error between the target and the predictions and passes the value to the training algorithm that minimizes it through interactively update of the weights θ.

2.7 Model Prediction and Validation

After the preceding steps, it is expected to have, at least partially, a particular model that is capable to describe and predict the system. However, it remains to test if the predictions of the model are useful. This evaluation involves various metrics and procedures to assess qualitatively and quantitatively how the model performs, this is known as validation. With those in hand, one can reject or approve the model, knowing that a model is never a final and true description of a system and can always contain a degree of inaccuracy. This means that the model must suffice a purpose, as a perfect model is philosophically impossible [17].

To this end, a common practice in validation is to split the data or use a totally different data set, with different inputs from the estimation. This ensures that the tests in the validation phase are as independent as possible. Although for chaotic systems, that are very sensitive to the initial conditions, this approach may not be appropriate [27].

First, one must know that the prediction can be made in different ways. The One-Step-Ahead (OSA) approach uses the measured values, contained in the dataset, for the prediction of one time-step ahead of the output. It should be noted that the model can be biased and the OSA prediction can mislead to a false impression of a good model [27]. As such, it is not a good practice to analyze the adherence of the model over the course of the OSA Prediction. Assuming a linear system with noise, and that the initial conditions are known, the OSA prediction can be calculated according to [17], by:

$$\hat{y}(t|t-1) = H^{-1}(q)G(q)u(t) + 1[1 - H^{-1}(q)]y(t) \tag{2-28}$$

where $\hat{y}$ is the predicted value, $G(q)$ is a transfer function from input to output and $H(q)$ is analogous to $G(q)$ but from noise to output. For unknown initial conditions, when the data between an arbitrary time 0 and $t-1$ is available, the simplest approach would be to replace the unknown data with zeros [17].

As an example, considering the Dynamic ANN models in Section 2.6, the OSA prediction can be calculated in batch by using Equation 2-14.

Another type of prediction is the Free-Run Simulation (FRS), also called the Model Predicted Output. It uses a few measured values solely to

initialize the model. New predictions are calculated based on past predictions. Compared to the OSA approach, where the calculations are almost reset each step, suppressing the build-up of errors, on the FRS approach those tend to accumulate over time, better reflecting the real model capability of representing the system dynamics [27]. On the other hand, the FRS is more complex to calculate, assuming a generic ARX model, it is necessary to iteratively construct each regressor using past predicted data, which is based on the number of samples in the validation data set, which can be time-consuming. As such the first predictions from the measured input-output data are initialized so that:

$$\begin{cases} \hat{y}(1) = y(1) \\ \hat{y}(2) = y(2) \\ \vdots \\ \hat{y}(n_y) = y(n_y) \end{cases} \tag{2-29}$$

And then future predictions can be performed interactively by:

$$\begin{cases} \hat{y}_s(n_y+1) = & F(\hat{y}_s(n_y), \hat{y}_s(n_y-1), \ \dots \ , \hat{y}_s(1), \\ & u(n_u), u(n_u-1), \ \dots \ , u(1)) \\ & \vdots \\ \hat{y}_s(t) = & F(\hat{y}_s(t-1), \hat{y}_s(t-2), \ \dots \ , \hat{y}_s(t-n_y), \\ & u(t-1), u(t-2), \ \dots \ , u(t-n_u)) \\ & \vdots \end{cases}$$

where $\hat{y}$ is the predicted output value.

2.8 Validation Metrics

All the metrics presented can be applied for either OSA or FRS prediction. One must be aware that, if a model has poor performance in the OSA prediction, according to the metrics, in the FRS prediction it will still not perform [27].

The simplest evaluation metric is the residuals. It can be thought of as the "leftover" from the modeling process, which means that it contains the data the model could not reproduce [17]. It can be calculated by:

$$\xi(t) = y(t) - \hat{y}(t) \tag{2-30}$$

where $y(t)$ is the real value and $\hat{y}(t)$ is the predicted value.

If the model is truly unbiased, the residuals should form a white noise, meaning that all predictable information should have been captured [27]. A first visual inspection of the residual, at an appropriate scale, can help identify some problems that might have got through the preprocessing, such as outliers, drift, and others, discussed in Section 2.3. One must be aware that if the dataset is too short it is not possible to make a firm statement if some peculiarities such as drift and periodicity are truly present in the data or introduced by a ill model [18]. Also, even if the amplitude of the residuals is large, it is not a clear sign of a bad model, as it could indicate a poor noise-to-signal ratio due to faulty sensors or even bad experiment design [27].

Based on the residuals, other metrics can be calculated. An example is an error quantitative metric by applying the equation 2-27 to the residuals. However, complex models with several parameters naturally tend to have lower MSE for both linear and nonlinear cases. As such, only the MSE is not sufficient to properly judge a model as it can have a good MSE, but it can be biased toward the fitted data and have poor generalization for new data sets [27]. In summary, the model is overfitted towards the training data and it can be identified trough validation with different datasets from the estimation phase.

Another error quantitative metric based on the residuals is the multiple correlation coefficient or R^2 in short. Compared to the MSE, it lacks the dependence on the amplitude and it is calculated by:

$$R^2 = 1 - \frac{\sum_{t=1}^{N} [\xi(t)]^2}{\sum_{t=1}^{N} [y(t) - \bar{y}]^2} \tag{2-31}$$

where values closer to one means a better fit of the model.

Additional statistical properties of the residuals or based on other metrics can be useful. In the case of the MSE, they tend to alleviate the aforementioned problems but usually assume that the residuals have normal or Gaussian distribution, which for nonlinear systems is not always true [27].

Assuming that the residuals should not correlate linearly or non-linearly with any combination of past inputs or outputs, correlation tests of the residuals can help to quantify its white-noise condition and model validity [81,82]. As such, assuming that the residuals are equal to $\xi(t) = y(t) - \hat{y}(t|t-1)$, where $y(t|t-1)$ is the OSA prediction, the residuals are truly white noise, or unpredictable, when the following statement is true:

$$\begin{cases} \phi_{\xi\xi}(\tau) = \delta(\tau), \quad \forall\tau \\ \phi_{u\xi}(\tau) = 0, \quad \forall\tau \\ \phi_{\xi(\xi u)}(\tau) = 0, \quad \tau \geq 0 \\ \phi_{(u^2)'\xi}(\tau) = 0, \quad \forall\tau \\ \phi_{(u^2)'\xi^2}(\tau) = 0, \quad \forall\tau \end{cases} \tag{2-32}$$

where $(u^2)' = (u(t))^2 - \bar{u^2}$, $\xi u = \xi(t+1)u(t+1)$ and ϕ is the Cross-correlation between two signals x and y defined as:

$$\phi_{xy}(\tau) = \frac{\sum_{k=1}^{N-\tau}[x(t) - \bar{x}][y(k+\tau) - \bar{y}]}{\sqrt{\sum_{k=1}^{N}[x(t) - \bar{x}]^2}\sqrt{\sum_{k=1}^{N}[y(t) - \bar{y}]^2}} \tag{2-33}$$

where an upper bar, like $\bar{x}$, denotes the mean value of a sequence.

3
Case Studies

Both case studies, namely respectively, Piezoelectric micromanipulators and Piezoacoustic transmission, use PEA as the main element of excitation of the system. Although the objectives of those systems are different, the presence of nonlinearities such as hysteresis and creep inherent to piezoelectric materials are present. Additionally, both systems are subject to their own complex dynamic originated from their respective applications, further increasing the modeling difficulty. As an example, the acoustic transmission case can have more variables to manage due to multiple interfaces and materials while the micromanipulator has fewer variables but needs to be fast, repeatable, and precise in a narrow displacement range and higher loads.

3.1
Piezoelectric Micromanipulator

The goal of the experiment is to simulate a 1-DOF piezoelectric micromanipulator and study the hysteric behavior of the piezoelectric element when subjected to different operational conditions like differences in stimulus signal frequency. A test bench, exhibited in Figure 3.1, was developed. It consists of a PEA with a cantilever structure of rectangular section of two layers, one of which is based on lead-zirconate-titanate piezoelectric material and the other one is based on non-piezoelectric layer. The overall dimensions are (length, width, thickness): 15mm x 2mm x 0,3mm. Which is classically used in micromanipulation applications with 1-DOF.

Additional equipment necessary to generate the arbitrary electrical signal, and to measure the displacement, was included to ensure reliable data acquisition and easier change of parameters. Such as a computer using Matlab Simulink and a power amplifier to stimulate the piezoelectric element with an arbitrary input voltage u spanning from $[-100, 100]$ V. And an optical displacement sensor, having a resolution of 10nm and a bandwidth of 5kHz (LK2420 from Keyence) to measure the deflection of the cantilever beam y. All data was acquired and converted with an acquisition board (dS1104 from dSPACE) set at a 10kHz sampling frequency. The high sample rate used is important for this application, for rapid and accurate micropositioning.

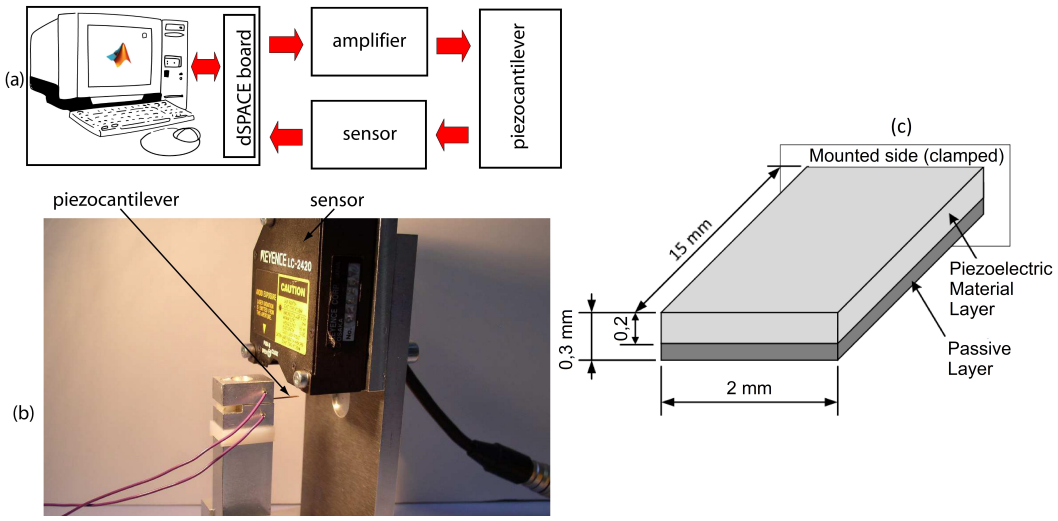

Figure 3.1: Description of the piezoelectric micromanipulator actuator test bench. A voltage is applied to the active layer of the beam, which deflects due to the piezoelectric effect. (a) MATLAB and dSpace are used to send the input commands and store the data for identification which is performed offline. In (b) we show the real system where the acquisitions were made. And in (c) the dimensions and layers of the piezoelectric micromanipulator.

As shown in Figure 3.2 the objective is to develop a model capable to compensate the hysteresis inherent to the system and the piezo cantilever micromanipulator. This can be done with or without feedback. The last provides online update capabilities to the model and can accommodate changes in the setup, such as the change of the piezo cantilever. The first approach, with no feedback, is compared to a calibration, as once the system is changed, the model needs to be retrained with new data.

To this end, two signals were created. For estimation (i), the multisine signal and, for validation of each of the hysteresis modeling (ii), a pure sinusoidal. The multisine was chosen because it is a general-purpose excitation signal that can be designed to operate at a predefined frequency band of interest and amplitude. Which in this case was up to 0.5 kHz frequency and maximum amplitude of 100 V, as limited by the device. It has been constructed with $n_f = 5000$ sinusoidal signals and uniformly distributed with random phases. This band was chosen because it includes both the operating frequency range and the first resonant frequency of the PEA. Figure 3.3 shows the whole dataset (i) used for the estimation of the parameter.

Figure 3.4 shows the power spectrum of the excitation signal and the output of the system, spanning the band of interest. The peak around 750 Hz is outside the generated signal frequency band. Its presence may be due to nonlinearities or unknown disturbances. As this peak is closed to -20 dB,

compared to the base amplitude of 40 dB for the band of interest, this peak is disregarded as it is not interesting to analyze outside the excitation signal band.

For validation, several pure sinusoidal signals, one at a time, with different frequencies ranging from 0.1 Hz to 500 Hz, were used. This allows to evaluate the adherence of the model in capturing the behavior at several frequencies, which is a major issue for the piezo cantilever in micropositioning tasks.

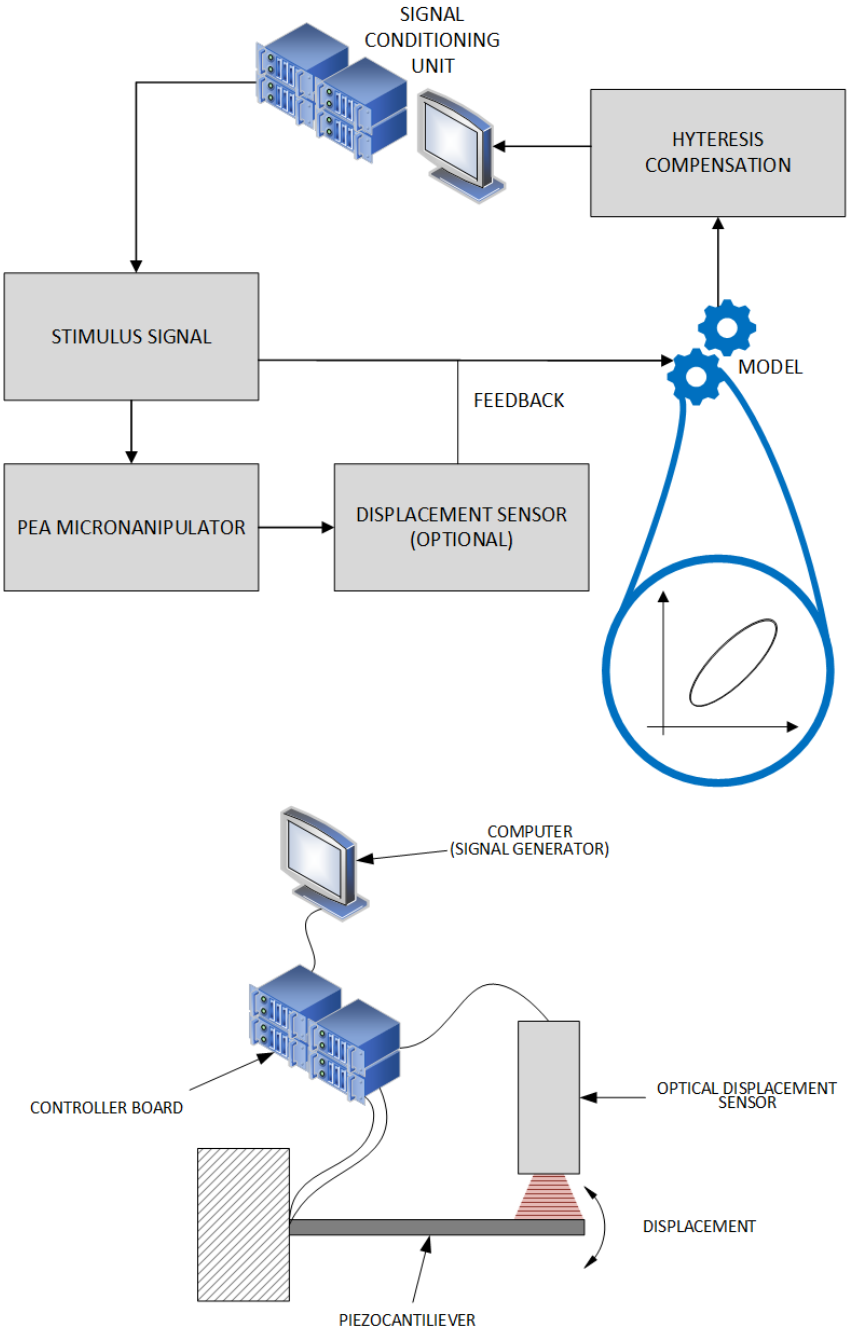

Figure 3.2: Proposed application of the technique to compensate the hysteresis inherent to the PEA for the Piezoelectric Micromanipulator.

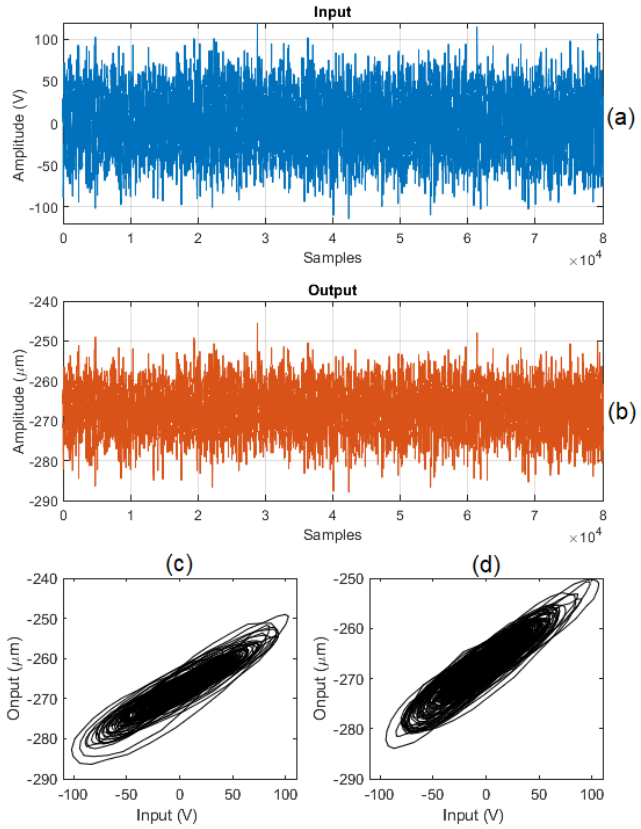

Figure 3.3: Exploratory plots of the measured input and output data for piezoelectric micromanipulator. In (a) the input [V] and (b) output [μm] of the whole dataset with eight seconds (8×10^4 samples at 10 kHz). And five thousand samples from zero in (c) and eight seconds in (d) from the input and output relations.

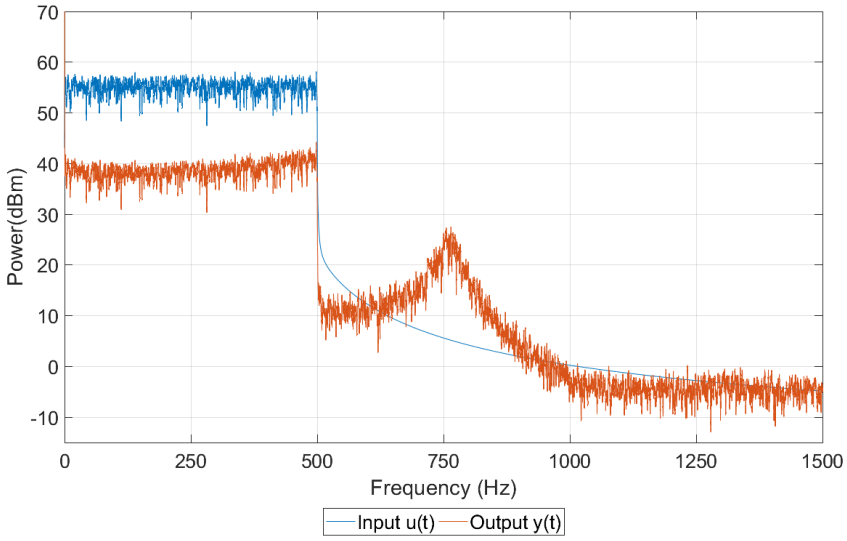

Figure 3.4: Power spectrum for the multisine input and the measured output for piezoelectric micromanipulator.

3.2 Piezoacoustic Transmission

The goal of this experiment is to simulate a piezoacoustic application with one piezoelectric transmitter (Tx) and receiver (Rx). The test bench can be visualized in Figure 3.5 and it is composed of:

- Two PEA of rectangular section and dimensions of 70x25mm (length, width). Both are attached to stainless steel plates using epoxy resin as shown in Figure 3.6;
- An arbitrary Function Generator as the signal source (Tektronix AFG3022C);
- An Oscilloscope to capture all signals (Tektronix MDO3024);
- A Linear Broadband RF Power Amplifier to boost the signal to the transmitter (Electronics and Innovation 2100L);
- A stainless steel tank with an integrated heater (Lauda Alpha RA24).

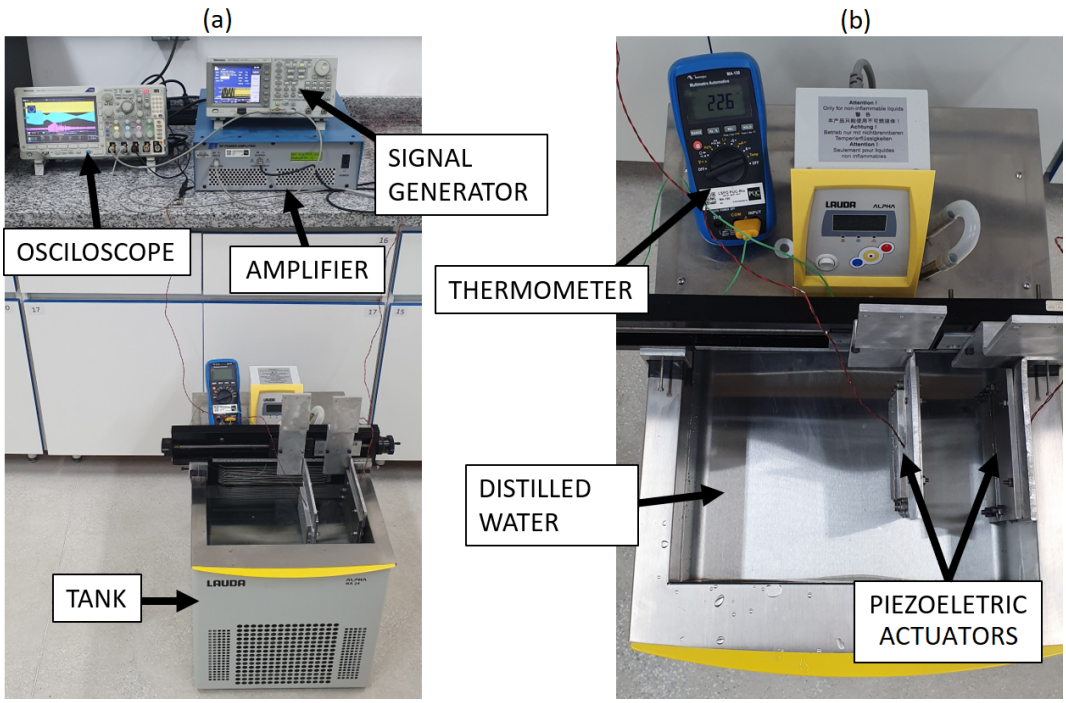

Figure 3.5: Experimental set-up description for the Piezoacoustic transmission case study. (a) Test Bench with an amplifier, oscilloscope, and signal generator; (b) Steel plates with PEA (on the lower right) at 10 cm away from each other. The tank is filled with distilled water at room temperature.

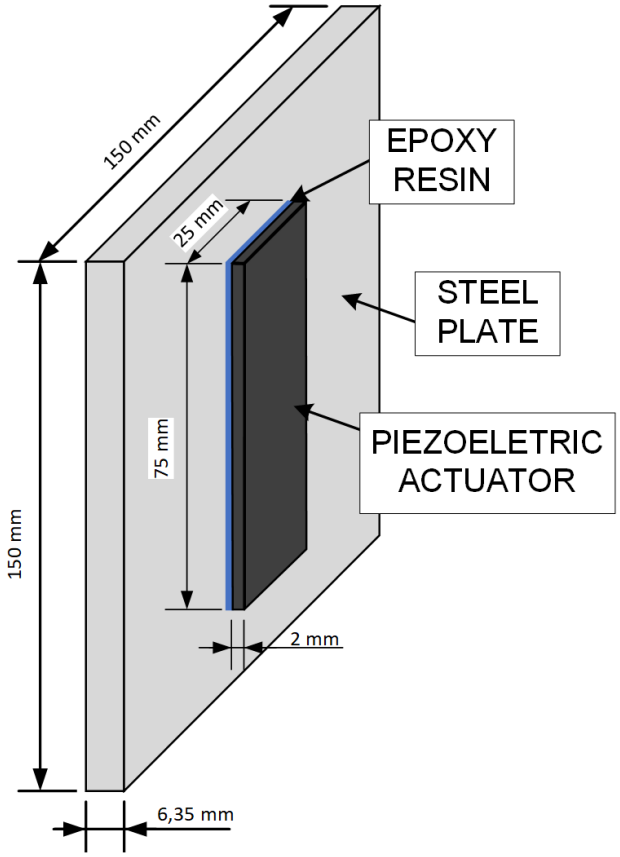

Figure 3.6: Schematic of the PEA bounded to the steel plate. Both Tx and Rx are identical and have the PEA bounded to the center of the steel plate.

As shown in Figure 3.7 the objective is to develop a model capable to identify the system optimal transmission frequency of data, energy or both simultaneously to a sensor in view of the presence of discontinuities in the medium and changes of the overall operational and ambient conditions. As those introduces undesirables reflections, the transmission efficiency degrades. As such, feedback from the Rx side is needed to perform the online update of the model, enabling the necessary modulation of the input signal. Moreover, the feedback can be performed trough the same acoustic channel of the transmission, as it function in both ways. However, in this scenario, additional circuitry is needed to separate the received and transmitted signals.

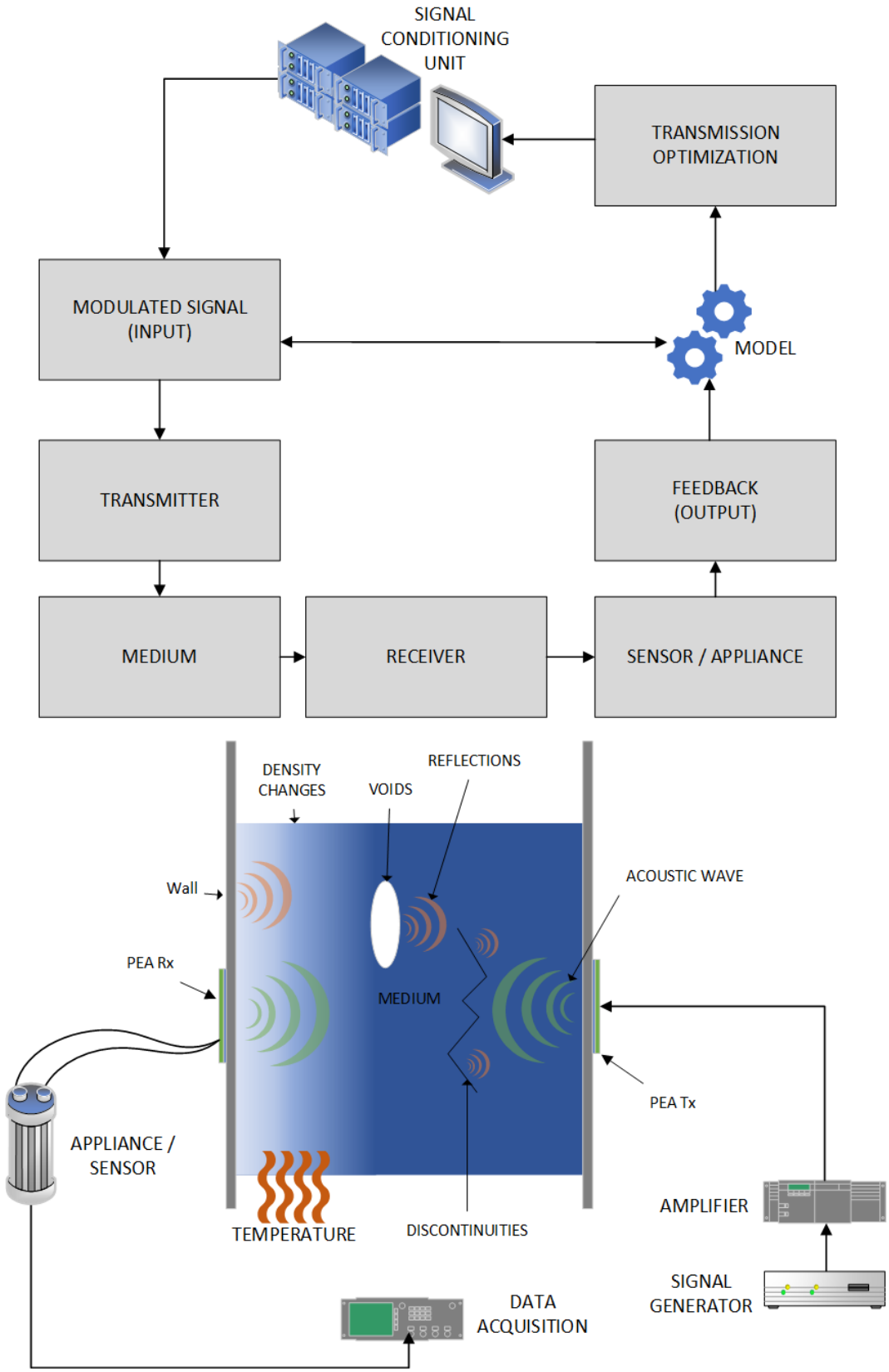

Figure 3.7: Proposed application of the technique to optimize and improve the transmission efficiency for the Piezoacoustic transmission case study.

The use of an power amplifier was needed because the signal generator can not create an arbitrary signal with sufficient amplitude for the PEA in this application. As the measurement of the amplified signal would not be possible with the available hardware, as a compromise, the data used as the input for the model was prior to the amplification. As such, the amplifier was made part of the system to be modeled as shown in Figure 3.8. Thus, any additional noise introduced by the power amplifier, which should be minimal due to the linear broadband nature of the specific equipment used, is considered in the modeling.

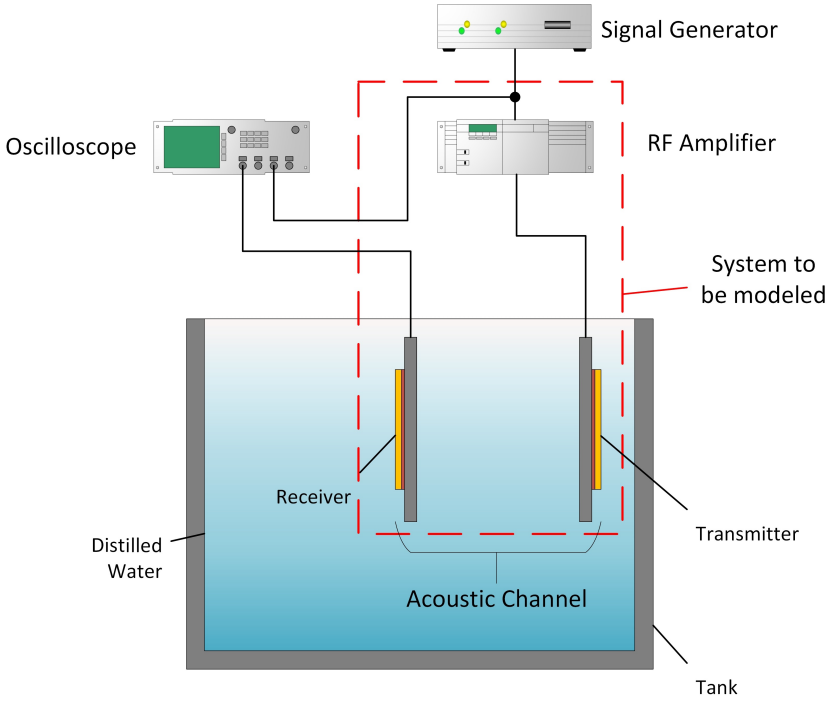

Figure 3.8: Schematic drawing of the system showing the input and output acquisition signals location for the Piezoacoustic transmission case study and the system to be modeled.

In this scenario, the four main variables that influence the dynamics of the system are: (i) the distance between the PEA, (ii) coupling fluid medium, (iii) temperature, and (iv) alignment between the steel plates (both in terms of the angle between them and the superposed area). Additional variables could be introduced through solid obstacles or discontinuities in the medium, induced by flow of gas or vibrations, as shown in Figure 3.7.

All these variables can lead to undesirable inner reflections and transmission losses, further complicating the modeling. In fact, those are present in real-world conditions, but due to the limited availability of equipment and time to model, a compromise between them was needed.

Considering this context, the variables were set as such: the Tx and Rx actuators spaced 100 mm and aligned concerning each other. The setup was skewed to the right side of the tank, meaning that the Tx was closed to the wall, as shown in Figure 3.5(b). This aims to reduce the inner reflections due to the size of the tank. Finally, the tank was filled with distilled water and kept at room temperature (24°C) and no additional obstacles or discontinuities were introduced.

Thus, the acoustic channels contain five layers and three materials (epoxy, steel, and distilled water) where both data and energy can transverse. Then, a Vector Network Analyzer (VNA), model Keysight E5061B, is used to excite the system with a 100ms swept sine signal of 707 milliVolts RMS, or 2V peak-to-peak. This aims to detect the band of interest of the device under test. This resulted in an increased response in the range between 900kHz to 1350kHz. Figure 3.9 shows the power spectrum of the input signal used by the VNA as a stimulus for the Tx PEA and the amplitude responses of the Rx PEA. Thus, indicating that the peak transmission is located at $\approx 940kHz$.

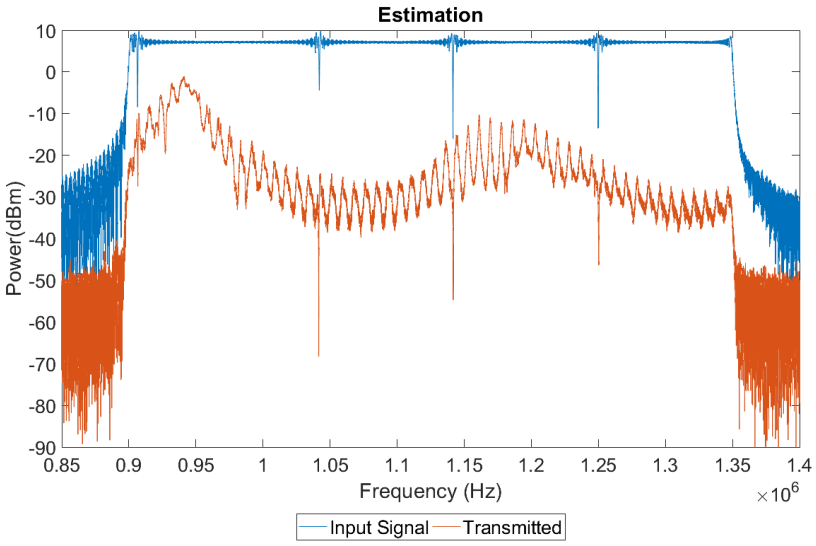

Figure 3.9: Power spectrum as measured by the VNA for the Piezoacoustic transmission case study. It is possible to see that the system has a peak in transmitted power at 940kHz with a second peak around 1162kHz.

The first dataset utilizes for the estimation a chirp signal. It was chosen due to its characteristic to excite the system in many frequencies, resulting in faster measurement rates and a higher SNR. The change rate of frequency was set as a linear function of time with 100ms of period and amplitude before amplification equal to 80mVpp. The frequency range was set from 900kHz to 1350kHz according to the VNA.

The data was acquired at a sample rate of 100MHz to capture the maximum amount of information of both Tx and Rx signals. This resulted in 10 million points for the 100ms period of the signal. On the other hand, the resulted dataset was oversampled. Therefore, it was necessary to preprocess the data before the estimation and resample it.

Instead of using the Nyquist-Shannon Theorem [63] to find the minimum-sampling rate at which a continuous signal can be recovered, the method proposed in [83] was used as a guideline to find the ideal sampling frequency. It consists in purposely oversampling the dataset and calculating the linear and nonlinear covariance functions. Then, it is determined the necessary decimation, and consequently the sampling frequency, based on the lag of each function. This resulted in a reduction of the total number of samples from 10 million to 1 million.

To further process the resampled data, the frequencies outside the band of interest were removed by a fifth-order band-pass filter. This new resampled and filtered dataset was truncated to 2000 samples for creating the models. Due to the characteristics of the signal, this new dataset does not contain the entire frequency range of the original signal, but the gain in performance allows us to obtain the model predictions for all orders tested. The input-output is shown in Figure 3.10.

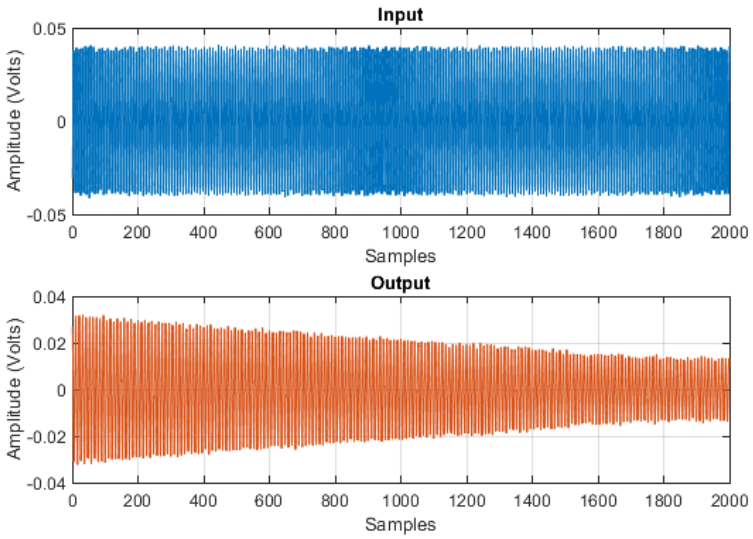

Figure 3.10: Input and Output, of the first dataset, used for the creation of the model for the Piezoacoustic transmission case study.

The second dataset utilized both an estimation and validation signal. For the estimation phase, it was employed the multisine signal and for the validation, the linear chirp. The multisine was chosen because it is a general

purpose signal that has an adjustable wide spectrum simultaneous stimulus and is easy to generate.

The multisine had a randomly sampled phase in the range $[0, 2\pi]$ with uniform distribution. The number of components was set at $n_f = 45,000$ which turned out to represent a reasonable resolution for the frequency range of 900kHz to 1350kHz, and 400mV amplitude. The original signal contained 1 million points. Limitations of the available memory of the signal generator, and the sampling rate needed to correct excite the system, limited the maximum number of points of the original signal that could be used. Therefore it was truncated to 5 thousand points. Due to the nature of the multisine, it would still cover the entire band of interest but with a lower resolution.

For the validation phase of the model, a linear up-chirp with a sweep time of 1 ms was used. That means it takes 1 ms for the signal to sweep the entire span of frequencies, which range from 900kHz to 1350kHz. The amplitude was set to 150mVpp. As it was natively created by the signal generator, no additional treatment of the signal was needed.

Similar to the first dataset, the data acquisition was performed at 100MHz sampling frequency, resulting in an oversampled dataset of 10 million samples for both estimation and validation signals that needed to be optimized.

This was achieved through a moving average filter, with a span of 100 points, that was used in both estimation and validation. Those were further re-sampled to 5 times the maximum frequency in the band of interest, which amounts to 6.75MHz or two and a half times the Nyquist sampling frequency needed to represent a signal with a maximum input frequency of 1350KHz. This resulted in a decrease from 10 million points to 27 thousand points without any noticeable loss in resolution in the frequency domain. This resulted in a loss of amplitude in the power spectrum, as shown in Figure 3.12 and 3.14. However, as a benefit from the preprocessing removed peaks outside the interest band, smoothing and de-noising both the Tx and Rx signals, as shown in Figure 3.11 and 3.13.

Nevertheless, due to the available tools, computational and memory limitations, the signal needed to be further reduced in size. This was accomplished by simple truncation of the data, resulting in 2 thousand points for the multisine (estimation) and 1 thousand points for the chirp (validation).

In the case of the estimation, due to the nature of the multisine, the signal still covers the entire band of interest but with a lower resolution. For the validation, due to the linear nature of the chirp, the signal kept the resolution but was a slice of the original band of interest. For the validation, it was not a problem since the truncation could be shifted and the model

validated for several slices of the range. For the estimation, this could pose an additional layer of difficulty to the modeling, but the gain in computation time was noticeable.

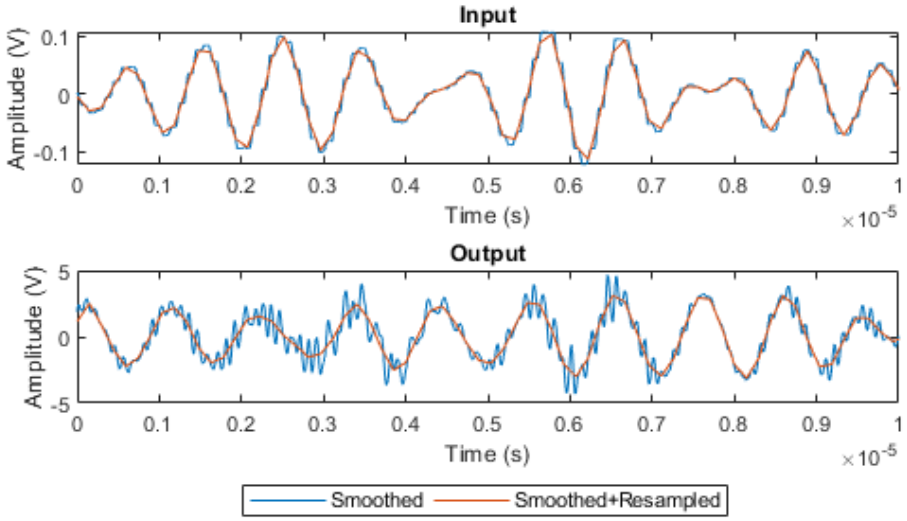

Figure 3.11: First 10 μs of the Multisine signal pre-process (estimation).

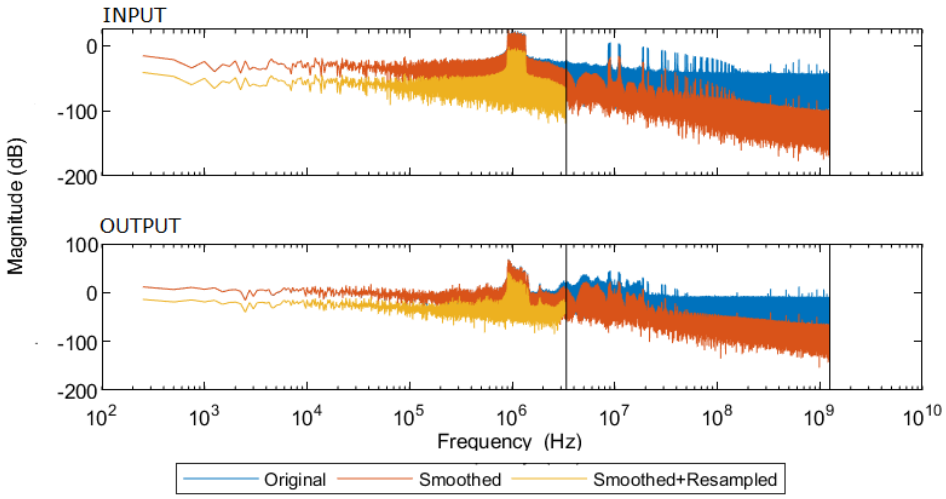

Figure 3.12: Power Spectrum comparison for the Multisine (estimation).

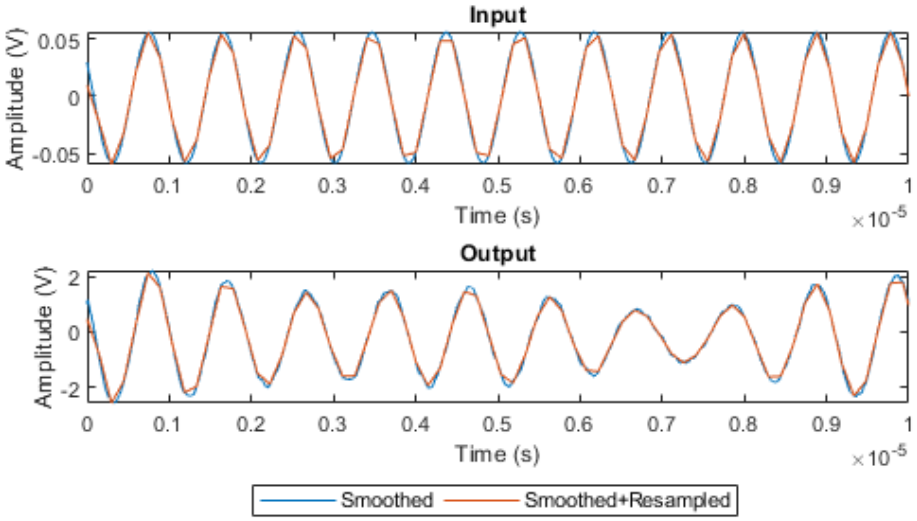

Figure 3.13: First 10 μs of the Linear chirp signal pre-process (validation).

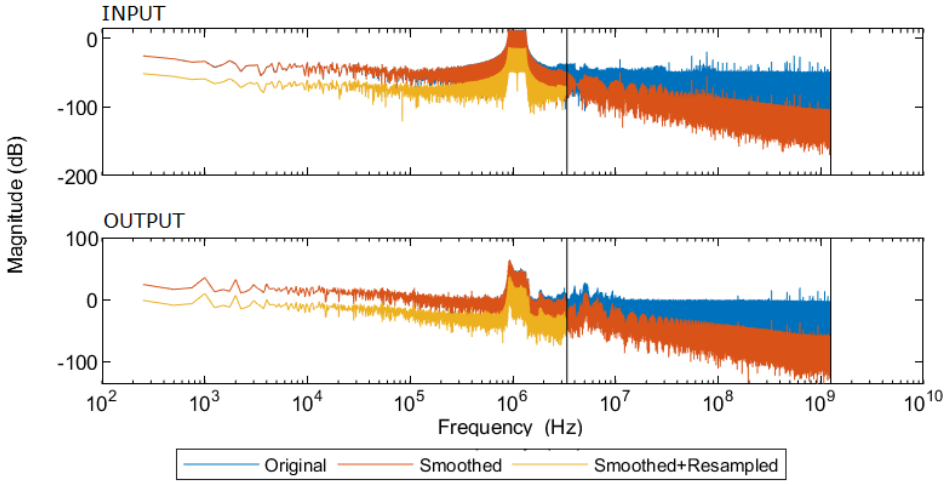

Figure 3.14: Power Spectrum comparison for the Linear chirp signal (validation).

Part II

Contributions

4
Piezoelectric Micromanipulators

A PEA, with a cantilever structure and rectangular section, is employed for a 1-DOF micromanipulator application. A general-purpose signal is used to capture the dynamics of the system in the interest band. Several ANN architectures are tested and compared based on validation metrics. The best one is validated through several pure sinusoidal to verify the model adherence in several frequencies. The results show that this contribution is suited for predicting hysteresis loops of piezoelectric based micro-manipulators.

4.1
Results for Deep Learning Applied to Data-driven Dynamic Characterization of Hysteretic Piezoelectric Micromanipulators

Both estimation (training) and validation datasets were normalized and the results are given in a dimensionless scale. The model of choice was an ANN and the training parameters can be visualized in Table 4.1.

Table 4.1: Parameters used for creation of the ANN models for the Piezoelectric micromanipulator case study.

Description	Value
Training algorithm	RMSprop
Loss function	MSE
Epochs	100
Learning rate	10^{-4}
Batch (input/output pairs)	128
Activation function	ReLU
n_y order	10
n_u order	10
N° hidden layers	[3-5]
N° neurons per layer	[25,50,100]
Architecture Type	Feed-forward

The convergence of the loss function MSE, during the training phase, occurred during the first epochs for most of the models. Little improvements were observed after the first 10 epochs, as shown in Figure 4.1. Therefore, indicating that the choice of training parameters were adequately selected.

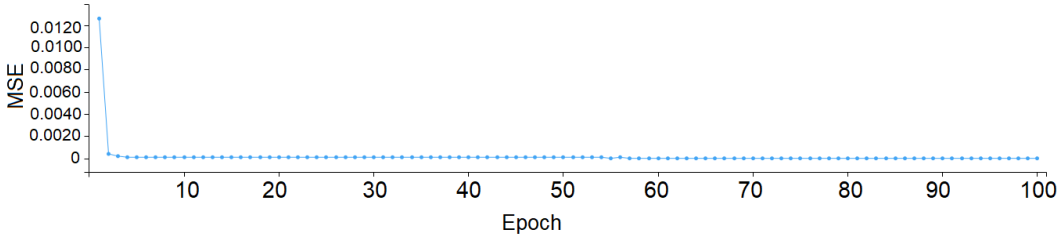

Figure 4.1: Convergence example of the loss function for the model with 4 layers of 25 neurons.

Table 4.2 summarizes all tested architectures in validation. To choose the best model the criteria took into consideration the mean values R^2 of the FRS prediction in the estimation and validation phase, the total number of parameters, the MSE and the complexity of architecture.

Table 4.2: Mean of the values of R^2 for all validation datasets and total number of parameters, according to the different architectures tested.

Layers	Neurons	Mean R^2	Parameters
3	25	0.984742017	1851
3	50	0.992217724	6201
3	100	0.964782331	22401
4	25	0.989210717	2501
4	50	0.916190505	8751
4	100	0.992844673	32501
5	25	0.992375649	3151
5	50	0.986898346	11301
5	100	0.992068821	42601

Between the candidates, the model with 4 layers of 25 neurons, totaling 2501 parameters, was chosen as it presents a better compromise between complexity and accuracy. One might say, at first glance, that the model with 5 layers of 25 neurons, totaling 3151 parameters, is better. But it provides approximately a 3% increase in R^2 for 26% more parameters. Also, as shown in Figure 4.2 the mean of the MSE during the training phase was lower for the chosen model.

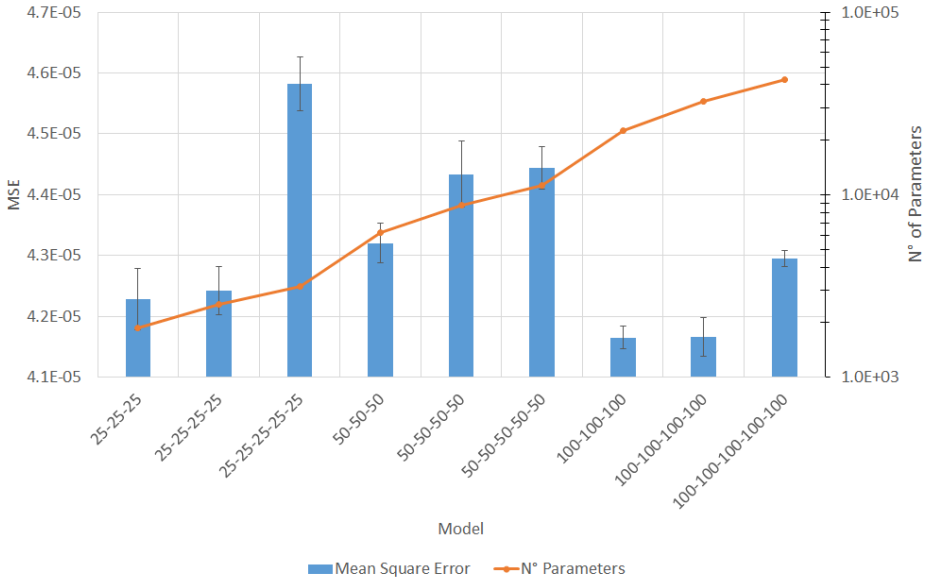

Figure 4.2: Comparison between the models for the loss function (MSE) and the number of parameters.

It is possible to see a pattern in Figure 4.2 regarding the number of hidden layers and the loss function. Except the model with 50 neurons, the models with 5 hidden layers performed far worse than its 3 and 4 layers counterparts. This is an indication of an overfit, where the increased complexity of the model leads to a very close representation of the training data, but poor generalization over the new data presented in the validation. Also, the models with 100 neurons had smaller overall deviation, indicated by the error bars, compared to other models.

In Table 4.3 the validation of this model with respect to R^2 obtained for each sinusoidal is detailed. The values are close to unity, showing the excellent prediction capability of the constructed model.

Table 4.3: Values for R^2 in validation phase, varying frequencies for the excitation signal, using 4 layers of 25 neurons.

Frequency (Hz)	FRS	Frequency (Hz)	FRS
0.1	0.986797839	200	0.994559081
1	0.989170955	250	0.985648806
10	0.991136621	300	0.995859260
50	0.998469432	400	0.987992324
100	0.998403016	450	0.997331124
150	0.997474415	500	0.985664909

By plotting the predicted value with respect to the real value we confirm the obtained R^2 and further inspect the results. Figure 4.3 shows that the lines of prediction and measured data are almost superimposed. Additionally, the shape of the loops curves changes with the frequency. This indicates that the hysteresis is influenced by the excitation signal frequency, as expected, and compensation needs to be employed in those cases.

Furthermore, under specific frequencies, such as 200, 250, 400, and 500Hz, the results show larger spaced intervals. This could lead to improvements in the design of the experiment as one might conclude that for higher input frequency scenarios, the sampling rate needs to be even faster.

The results have shown that deep neural networks have the potential for dynamic modeling of PEA in micromanipulator applications. Also, the use of several pure sinusoidal for validation provided insights into the model adherence and the hysteresis. The high accuracy model obtained for this application allows the prediction of the hysteresis based on the input signal frequency.

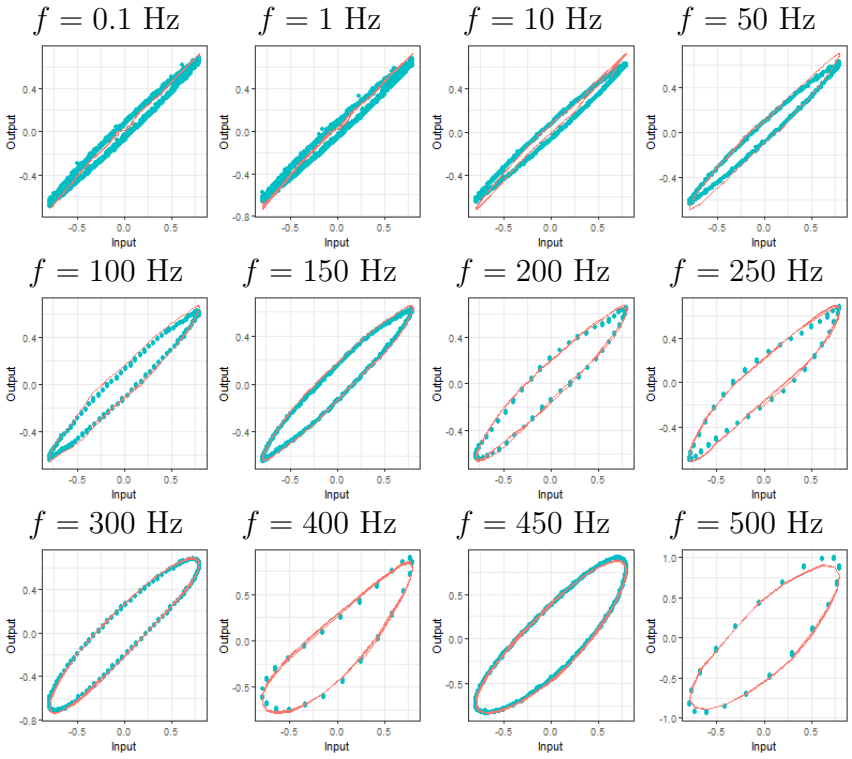

Figure 4.3: Output predictions for the selected model for the piezoelectric micromanipulator case study. Note that the data is normalized. Curves of $u(t)$ versus $y(t)$ (blue) and $\hat{y}_s(t)$ (red) for the various frequencies tested in validation phase. Note that the hysteretic behavior has been adequately captured for a wide band. Also, it is interesting to note how the hysteresis loop shape changes when the frequency increases.

5
Piezoacoustic Transmission

A test bench was developed with two PEA submerged in distilled water to simulate an acoustic transmission application, enabling reliably and fast data acquisitions. A survey of different data-driven modeling approaches were performed. A total of three models were tested and compared. They were the ARMAX with PEM estimator, the NARMAX with FROLS for the term selection, and the NARX with a ANN as the nonlinear function. Both OSA and FRS predictions were performed. A general purpose signal was employed for estimation and the models were not validated through a separated dataset. Instead, its quality was measured through metrics such as residuals and the R^2. Thus, each model was analyzed separately and summarized according to the ascending order of R^2 in FRS. The parameters used for the models were defined empirically and the results show that the most complex model (NARMAX) had the best accuracy, encouraging further creation of nonlinear mathematical data-driven abstractions for the piezoacoustic transmission application.

Additionally, an in-depth exploration of ANN models was performed to investigate how its architecture and parameter changes affect the model prediction. This also used a general purpose signal for estimation of the several thousands of configurations tested. Then they are compared based on residuals and quantitative metrics. The eight most accurate models were validated with a linear chirp signal. To account for the stochastic nature of ANN models, each architectures were validated multiple times. The best overall architecture was then further validated a total of 75 times to provide more insights on its performance. Although the results do not have a perfect fit for the validation data, it serves as a proof of concept for the use of ANN for this specific application.

5.1 Results for Evaluation of Nonlinear System Identification to Model Piezoacoustic Transmission

The parameters used for the estimation of each model can be seen in Table 5.1. As shown, several configurations were tested and the best configuration is devised below.

Table 5.1: Parameters used for creation of the models for the Piezoacoustic transmission case study.

Model	Parameter	Value
ARMAX	n_u order	[1-10]
	n_y order	[1-10]
	n_e order	[1-10]
NARX	n_u order	[1-20]
	n_y order	[1-20]
	N° hidden layers	[1-2]
	N° neurons per layer	[4-5,10]
	Architecture Type	Cascade-forward or Feed-forward
	Non-linearity estimator	Sigmoid or Wavelet network
NARMAX	n_u order	[1-10]
	n_y order	[1-10]
	n_e order	[1-10]
	n_l order	2
	ρ_p	$[10^{-4}, 10^{-6}]$
	ρ_n	$10^{-1}\rho_p$

For the ARMAX, the best result obtained used the following orders: $n_u = 2, n_y = 10$, and $n_e = 6$. The model error can be observed in Figure 5.1. Although the model does not include nonlinear terms, the obtained result presented good performance, with $R^2 = 0.9060$ in FRS.

For the NARX model, a higher fit value was obtained with higher total complexity. The model that obtained the higher R^2 in FRS used a sigmoid network as the activation function with the best model having the following orders: $n_u = 15$, and $n_y = 16$, with $R^2 = 0.8920$.

Comparing the residuals for both the ARMAX and the NARX models in Figure 5.1, the NARX error is greater on the center part of the dataset, while the ARMAX error is bigger in the extremities. This may suggest that an ensemble of both models may lead to a better overall fit.

The best models for the NARMAX model took in consideration not only the R^2 metric, but also the selected number of terms. As such, the chosen model has the following parameters: $n_u = 1, n_y = 2, n_e = 3$, $n_l = 2$, $\rho_p = 10^{-4}$, and $\rho_n = 10^{-5}$, with $R^2 = 0.9629$.

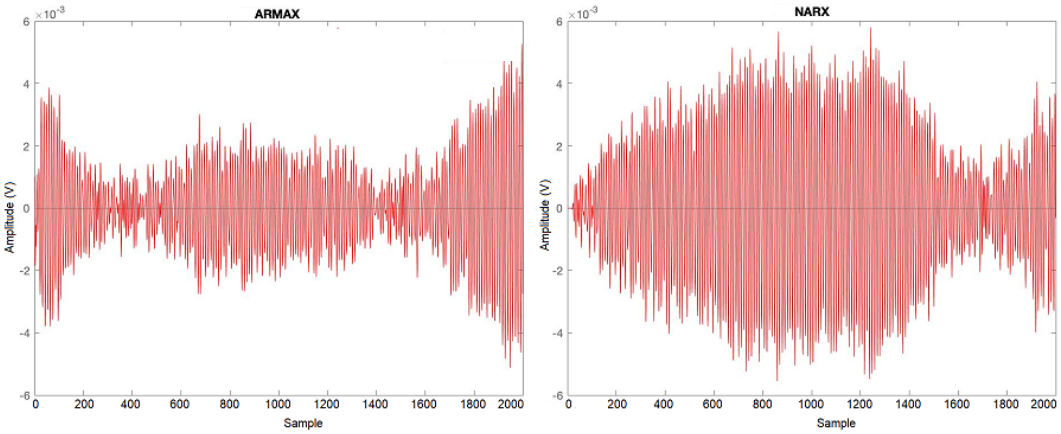

Figure 5.1: Residuals (error) for FRS prediction of the ARMAX (left) and NARX models (Right).

Figure 5.2 shows the scatter plot of the predictions vs. the measurements. It is possible to see that the point near the $0V$ mark has greater dispersion than the extremities. However, the fitted linear regression (green line) is close to the 45° slope (red line), which represents an ideal model.

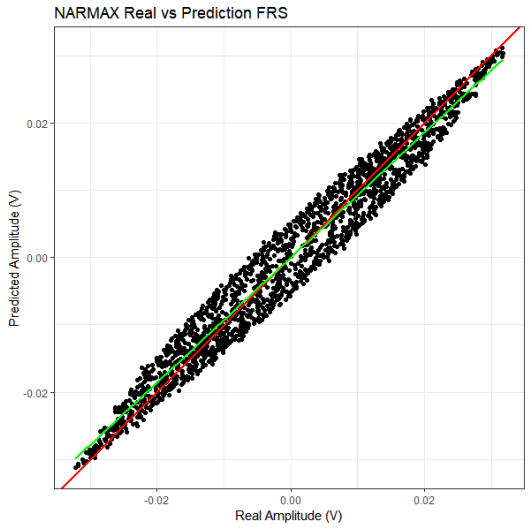

Figure 5.2: Measured vs Predicted for the free-run simulation of the best NARMAX model. In red the $y = x$ curve and in green the fitted linear regression for the predictions.

By comparing different prediction horizons and their respective residuals, Figure 5.3, the overall shape and amplitude between them are virtually the same. However, for the FRS in Figure 5.3(f), it shows a different pattern due to the FRS accumulation of errors over time and a greater amplitude when compared to the others prediction horizons. This further reassures the importance of the FRS prediction over the OSA and N-Step Ahead.

Additionally, one can see that both nonlinear models, NARMAX and NARX, have a similar pattern for the FRS residual but with different amplitudes. Further investigation is needed as this is not present in the linear model, ARMAX.

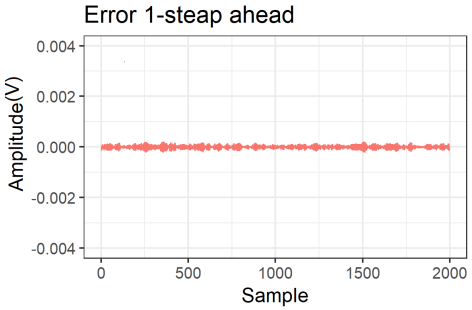

5.3(a): OSA Residual.

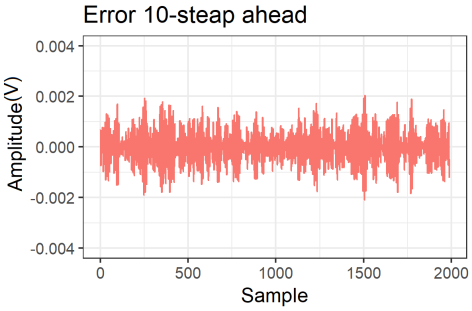

5.3(b): 10 Step Ahead Residual.

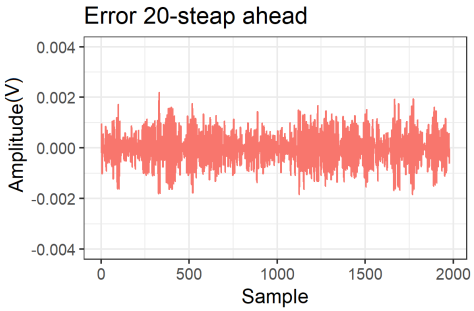

5.3(c): 20 Step Ahead Residual.

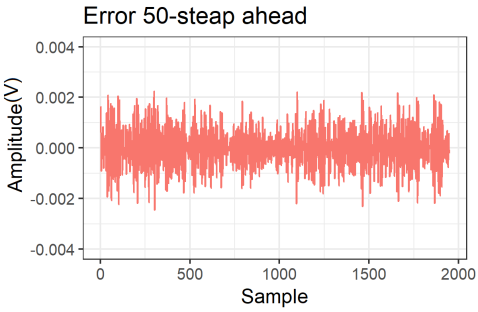

5.3(d): 50 Step Ahead Residual.

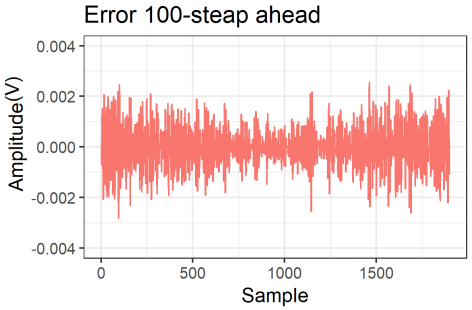

5.3(e): 100 Step Ahead Residual.

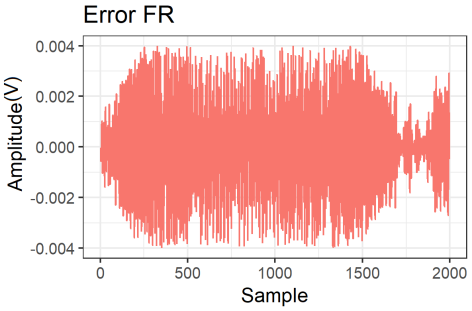

5.3(f): FRS Residual.

Figure 5.3: Residual (error) for the selected NARMAX model at different predictions horizons. Note that all plots have the same amplitude.

By comparing the residuals at the same horizons from Figure 5.3 in the frequency domain, as shown in Figure 5.4, its clear that the OSA residual has lower system dynamic left when compared to the others. Furthermore, the predicted output, $\hat{y}$, closes matches the peak at 950kHz of the measured output, y. Which according to Figure 3.9 is close to the peak transmission power of the frequency band of interest studied.

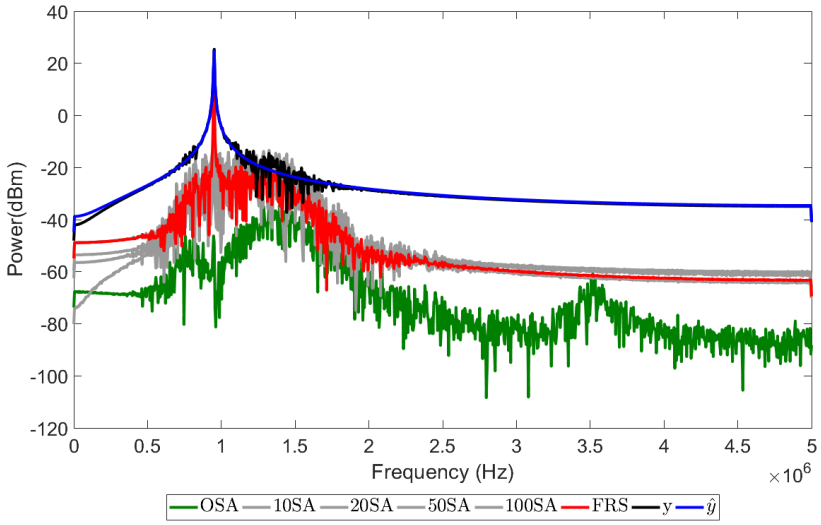

Figure 5.4: Frequency domain comparison between measured output y (black), predicted output $\hat{y}$ (blue), and prediction errors (residuals) at different prediction horizons. Note that the FRS prediction error is in red and the OSA is in green. All prediction in between those are colored in gray for clarity.

Still, the predicted output lacks some of the system dynamics on other frequencies that are outside the interest range. Note that the FRS residuals contains the most system dynamics of all residuals. This is expected as the FRS prediction tends to accumulate errors more easily. Furthermore, it has a peak that matches the measured output, indicating that the model did not capture the system dynamics completely.

This can be shown by plotting the residuals normal distribution in Figure 5.5. The OSA prediction residual has the narrower distribution and the FRS the wider.

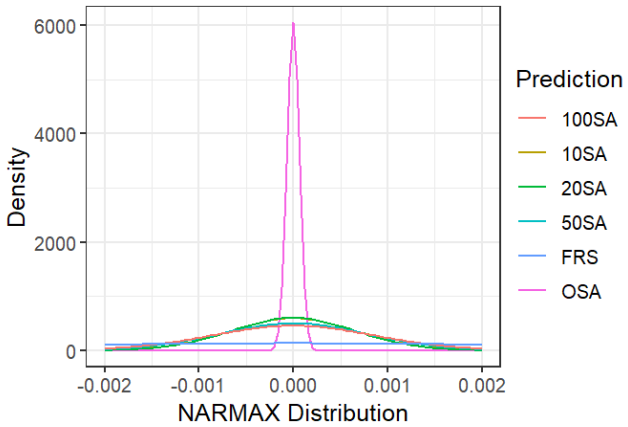

Figure 5.5: NARMAX residual (error) fitted normal distribution at different prediction horizons. Due to scale, the FRS distribution looks like a flat line.

Reinforcing the statement that the model did not capture all the system dynamics, both the auto-correlation of the residuals ($\phi_{\xi\xi}(\tau)$) and the cross-correlation between the residuals and the input vector ($\phi_{u\xi}(\tau)$) fall outside the confidence margins as shown in Figure 5.6. Meaning that there is still room for improvement.

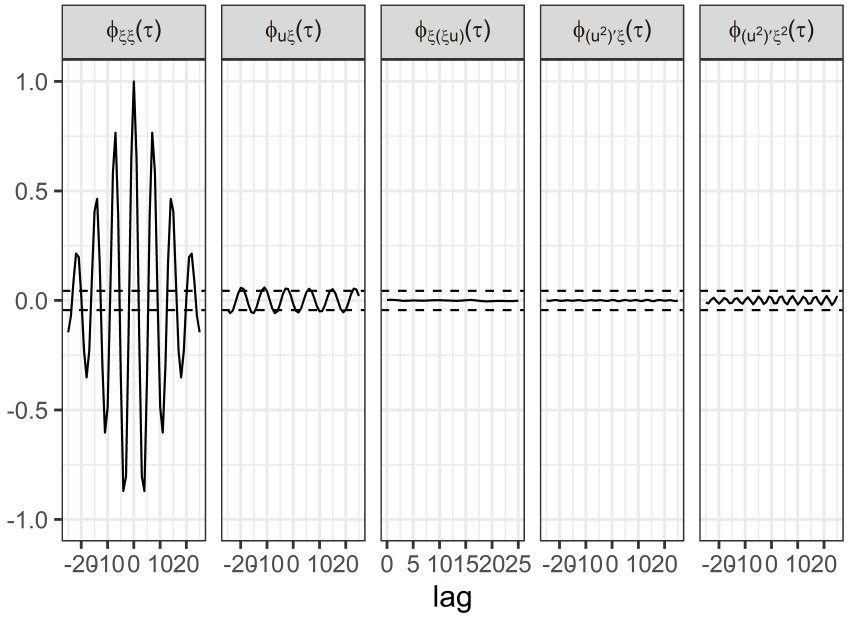

Figure 5.6: Correlations tests for the NARMAX model.

In Table 5.2 a summary of all tested models is shown in terms of R^2 in FRS. In this table, NARMAX had the best results, with a greater margin, when compared to the ARMAX and NARX. It is possible to see that the predictions are close to unity in FRS for the NARMAX case, which confirms this model's ability to represent the dynamics of the system using measured data.

As show in Figure 5.3, up to 100 steps ahead, the residual shape suffers virtually no change. By further investigating larger prediction horizons for the NARMAX model, one might find the sweet spot where the model starts to lose its accuracy for this system.

Table 5.2: Best models ordered by ascending order of R^2 in FRS.

Model	n_u	n_y	n_e	n_l	ρ_p	ρ_n	$R^2{}_{FRS}$
NARX	19	17	NA	NA	NA	NA	0.8830
NARX	17	16	NA	NA	NA	NA	0.8830
NARX	18	18	NA	NA	NA	NA	0.8880
NARX	15	16	NA	NA	NA	NA	0.8920
ARMAX	1	5	2	1	NA	NA	0.9000
ARMAX	1	5	5	1	NA	NA	0.9010
ARMAX	2	10	7	1	NA	NA	0.9040
ARMAX	1	8	3	1	NA	NA	0.9040
ARMAX	2	10	6	1	NA	NA	0.9060
NARMAX	1	3	1	2	10^{-4}	10^{-5}	0.9396
NARMAX	1	2	8	2	10^{-4}	10^{-5}	0.9612
NARMAX	1	2	3	2	10^{-4}	10^{-5}	0.9629
NARMAX	1	2	3	2	10^{-6}	10^{-7}	0.9651
NARMAX	4	5	10	2	10^{-6}	10^{-7}	0.9815
NARMAX	4	4	1	2	10^{-6}	10^{-7}	0.9819
NARMAX	4	6	4	2	10^{-6}	10^{-7}	0.9822
NARMAX	4	5	8	2	10^{-6}	10^{-7}	0.9824

5.2 Results for Evaluation of Deep Artificial Neural Networks for Data-driven Modeling of Piezoacoustic Transmission

The Keras package, in R language, was used to create the models, see [84]. Both estimation (training) and validation datasets were normalized and the training parameters for the ANN model can be visualized in Table 5.3.

As such, several hundred ANN configurations were tested with a input vector containing a minimum of 4 and a maximum of 2048 values from the input-output data. To account for the stochastic nature of ANN, each model was run twice and the best model, another 3 times. Meaning the results are the mean of 5 runs. The training algorithm used was an RMSprop.

For the majority of the models, the convergence of the loss function, during the training phase, occurred during the first 20 epochs, showing small improvements after the succeeding epochs, as shown in Figure 5.7. Additionally, the majority presented a smooth descent without spikes. As such, the parameters for the training phase were properly selected for the present models.

Table 5.3: Parameters used for creation of the ANN models for the Piezoacoustic Transmission case study.

Description	**Value**
Training algorithm	RMSprop
Loss function	MSE
Epochs	75
Learning rate	10^{-4}
Batch (input/output pairs)	128
Activation function	Sigmoid, ReLU, or tanh
N° hidden layers	[1-8]
N° neurons per layer	[2-10,16,25,32,50,64,75,100,128,256,512,1024]
n_u and n_y order	[2-10,16,32,64,128,256,512,1024]
Architecture Type	Feed-forward

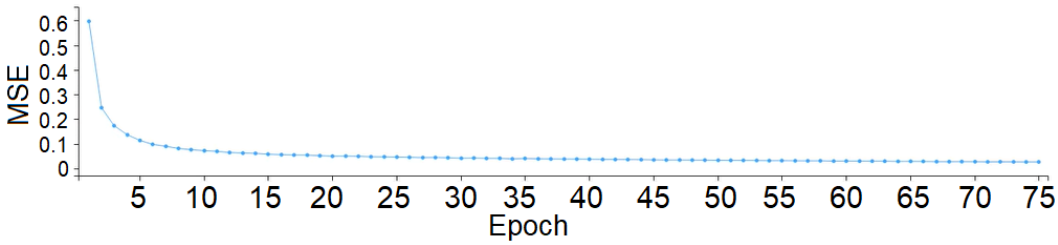

5.7(a): Example with less than 20 epochs until convergence.

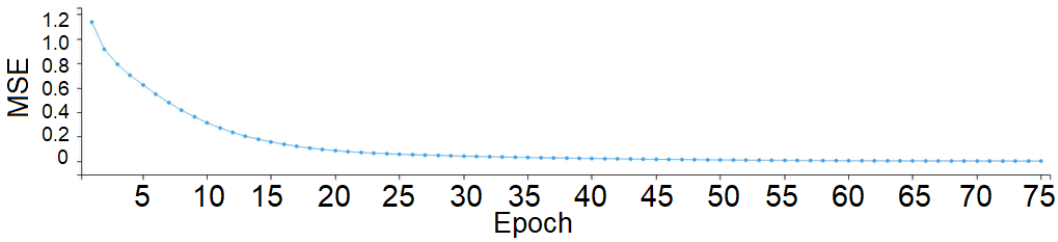

5.7(b): Example with more than 20 epochs until convergence.

Figure 5.7: Training examples with the selected parameters. The X-axis is the epoch number and Y the value for the loss function MSE.

Table 5.4 shows the best ANN models during the estimation phase. The choice of the best model took not only into consideration the mean of the evaluation metrics in both FRS and OSA, such as the residuals, cross-correlation tests, MSE, and R^2, but also the total number of parameters trained, for a better compromise between complexity and accuracy.

Table 5.4: Chosen ANN models, ordered by ascending value of R^2 during FRS in the estimation phase.

n_u	n_y	nrn	acf	${R^2}_{FRS_{MEAN}}$	${R^2}_{FRS_{SD}}$
1 - 512	1 - 256	256-128-64-32-16-8-4-2	tanh	0.9244	0.0292
1 - 512	1 - 512	256-128-64-32-16-8-4-2	tanh	0.9628	0.5274
1 - 512	1 - 512	100-100-100	tanh	0.9890	0.0043
1 - 512	1 - 512	50-50-50-50-50	tanh	0.9950	0.0014
1 - 512	1 - 512	50-50	tanh	0.9951	0.0025
1 - 512	1 - 512	50-50	sigmoid	0.9958	0.0015
1 - 512	1 - 512	100-100-100	sigmoid	0.9963	0.0016
1 - 512	1 - 512	75-75	sigmoid	0.9964	0.0015

Due to the number of architectures tested some insights could be extracted from the data. As an example, in Table 5.4, it is noticeable the absence of models with lower lags for n_u and n_y. Until lags of order 64 for both n_u and n_y, meaning 128 values for the input vector, there were no models with a good fit. This means that a higher number of past values are necessary for the correct prediction of this system. Moreover, the lack of models with $n_u \neq n_y$ does not mean that only models where $n_u = n_y$ had good accuracy. In fact, a lot of models with different lags had good results, but the majority of models with good fit had an equal amount of data from both input and output as the input vector for the ANN.

Another insight is that the majority of the good models had sigmoid and tanh as the activation function. Models with ReLU as the activation function resulted in poor performance, even in the estimation phase. This is a point for investigation as it is one of the most used functions and recommended given the limitations of the other two [74, 75].

Although the models provides an excellent fit for the estimation, they did not provide a good fit for the validation data in FRS, as shown in Table 5.5. Reinforcing the importance to validate a model with different signals.

The OSA simulation provided better results with an R^2 above 0.7 for all models, reaching 0.9 in some runs. This short prediction window, where the result has higher accuracy, could prove useful for some applications and control. Future works could extend this window to find exactly when the model loses accuracy, an example would be a 100 step ahead window.

Table 5.5: Chosen ANN models, ordered by ascending value of R^2 during FRS in validation phase.

n_u	n_y	nrn	acf	${R^2}_{FRS_{MEAN}}$	${R^2}_{FRS_{SD}}$
1 - 512	1 - 256	256-128-64-32-16-8-4-2	tanh	0.3841	0.2378
1 - 512	1 - 512	256-128-64-32-16-8-4-2	tanh	0.4204	0.2444
1 - 512	1 - 512	100-100-100	tanh	0.4341	0.0750
1 - 512	1 - 512	50-50-50-50-50	tanh	0.4383	0.1122
1 - 512	1 - 512	50-50	tanh	0.4950	0.0953
1 - 512	1 - 512	50-50	sigmoid	0.4977	0.2255
1 - 512	1 - 512	100-100-100	sigmoid	0.5281	0.0349
1 - 512	1 - 512	75-75	sigmoid	0.5642	0.0705

It is also noticeable that, by sorting in ascending order of R^2 in FRS, the models kept the same order between the estimation phase, Table 5.4, and validation, Table 5.5. This is not always the case as one model can provide great results in estimation but not in validation due to several factors such as overfitting, further reinforcing the importance of validation.

The best model according to all metrics and complexity, among all the chosen models, has 2 layers of 75 neurons each, sigmoid activation function, and 512 lags for n_u and n_y. Looking at each run in Table 5.6, the best run for this model had an R^2 of 0.6463 in validation. Considering the trade-offs due to the large bandwidth and sampling frequency required by the system, it is not a bad result.

Table 5.6: Individual runs for the best model, ordered by ascending value of R^2 during FRS in validation phase.

Run	${R^2}_{OSA_{EST}}$	${R^2}_{FRS_{EST}}$	${R^2}_{OSA_{VAL}}$	${R^2}_{FRS_{VAL}}$
1	0.9988	0.9971	0.8805	0.4729
2	0.9991	0.9981	0.8930	0.5110
3	0.9993	0.9965	0.8973	0.5916
4	0.9986	0.9941	0.8924	0.5991
5	0.9991	0.9962	0.9065	0.6463

This model was executed another 70 times, totaling 75 runs, to further analyze it. The evaluation metrics implies that there is still room to improve

this model. The residuals for the estimation phase in Figure 5.8, shows a peak in the same region in several runs for both OSA and FRS. Potentially indicating the presence of an outlier in the data.

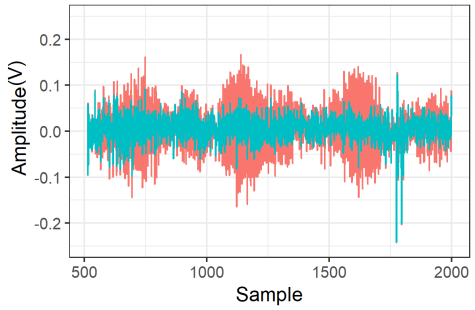

5.8(a): Run N°6.

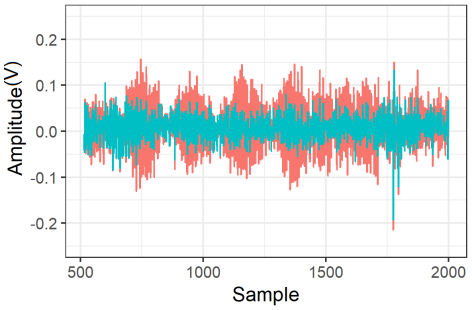

5.8(b): Run N°14.

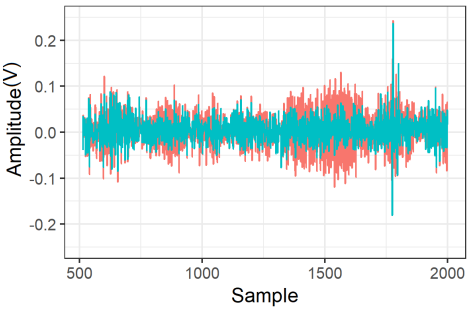

5.8(c): Run N°35.

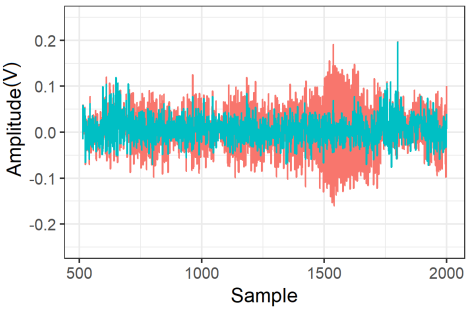

5.8(d): Run N°75.

Figure 5.8: Error (residuals) in FRS (red) and OSA (blue) predictions for the estimation (training) of the selected ANN model. Note that all graphs have the same amplitude in y axis.

The residuals for the validation phase, in Figure 5.9, have higher amplitude compared to the estimation, as expected based on Table 5.6. But the distribution of the residual is not as uniform, having a higher amplitude in the center region.

Selecting the run six and comparing both validation and estimation phases in the frequency domain we see that the validation has, as expected, lost its resolution due to the truncation, Figure 5.10. Additionally, the residuals still contains dynamic of the underling system, as both OSA and FRS predictions contains peaks near the 950kHz. Furthermore, outside the band of interest, there is a peak around 2750kHz. This could indicate that the model suffers from over-fitting or could indicate a source of noise that was captured by the model in the preprocess data. Those are not present for the estimation as show in Figure 5.11.

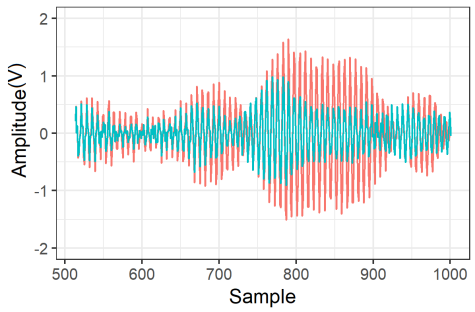

5.9(a): Run N°6.

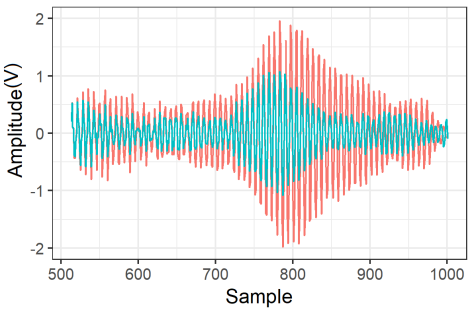

5.9(b): Run N°14.

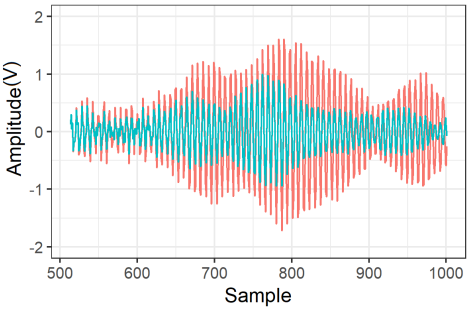

5.9(c): Run N°35.

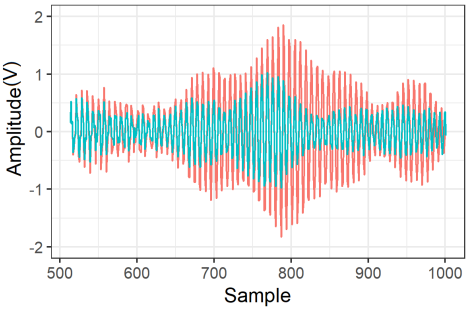

5.9(d): Run N°75.

Figure 5.9: Error (residuals) in FRS (red) and OSA (blue) predictions for the validation of the selected ANN model. Note that all graphs have the same amplitude in y axis.

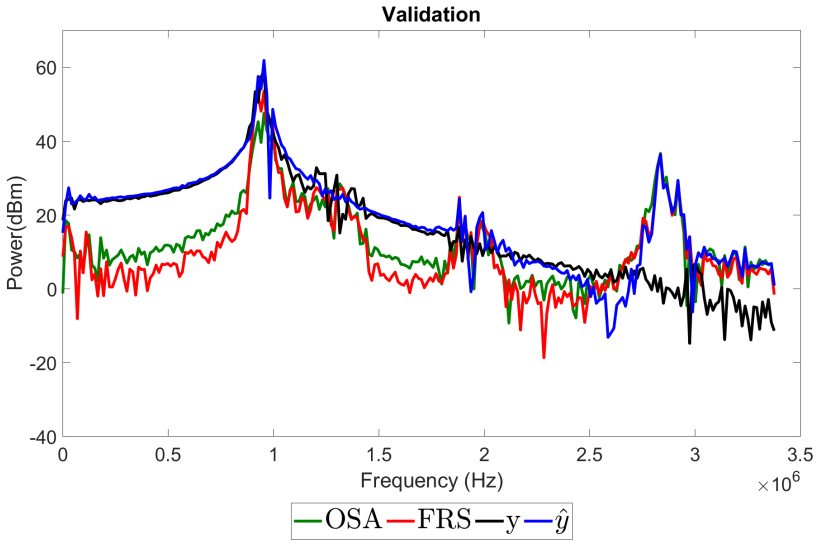

Figure 5.10: Frequency domain comparison for validation of run N°6 of the selected ANN model. In black the measured output y, in blue the predicted output $\hat{y}$, in green the OSA residual and in red the FRS residual.

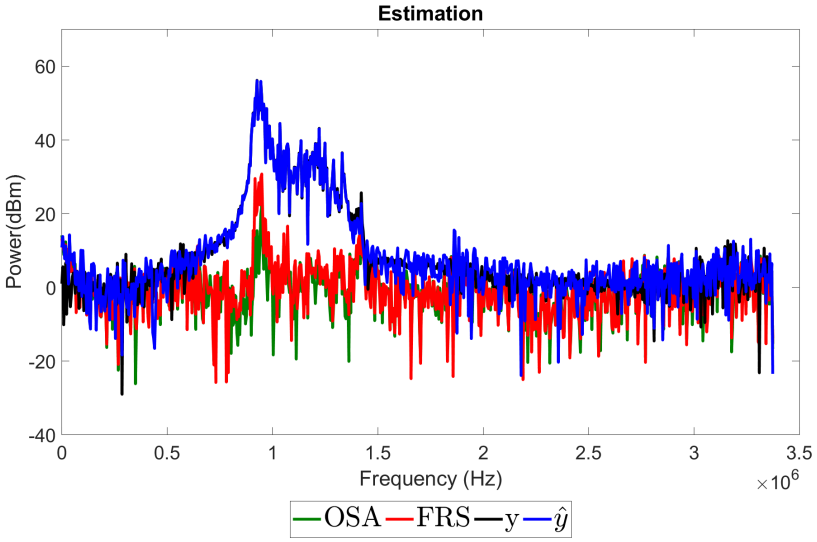

Figure 5.11: Frequency domain comparison for estimation of run N°6 of the selected ANN model. In black the measured output y, in blue the predicted output $\hat{y}$, in green the OSA residual and in red the FRS residual.

The scatter plot of the measured output by the predicted output, in Figure 5.12, shows that the estimation data is close to the ideal prediction, although that, at the extremes, the data points are distant from the fitted linear regression. The fitted linear regression for the validation data is still close to the ideal prediction, however the data point at the center is distant from it, as expected from Figure 5.9. This is a point for future work and maybe is connected to the data collection and/or preprocessing limitations of the case study.

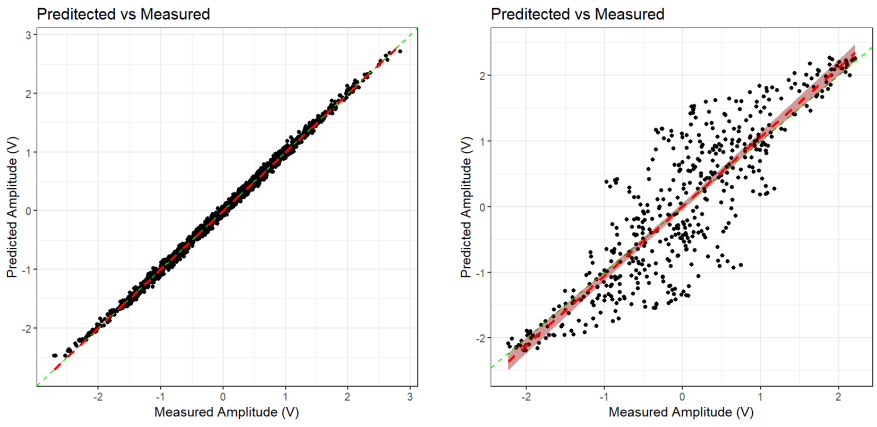

5.12(a): Estimation phase. 5.12(b): Validation phase.

Figure 5.12: Measured vs Predicted values in FRS for the selected ANN model structure. In green the x=y line and in red the fitted linear regression for the predictions.

Finally, the distribution of R^2, in Figure 5.13, shows that the validation result has higher standard deviation than the estimation. As the results of the validation are clearly inferior, further investigation is needed for the phase information of the signals. Those can be evaluated by plotting the measured output from the system versus the signals obtained using the FRS prediction.

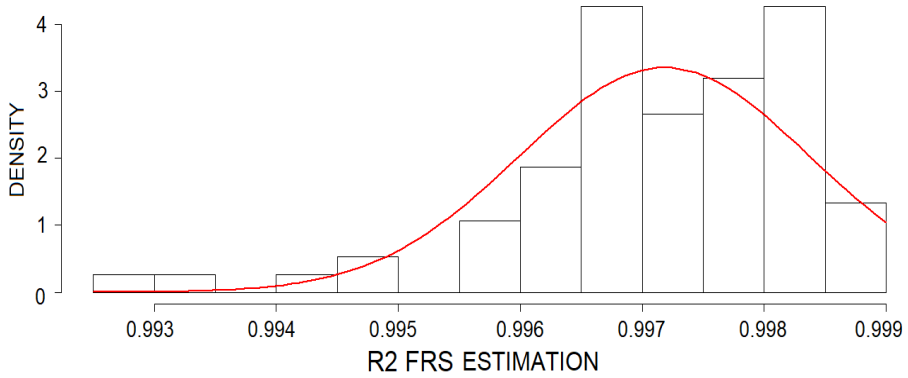

5.13(a): Estimation phase with mean 0.997181545 and SD 0.001188647.

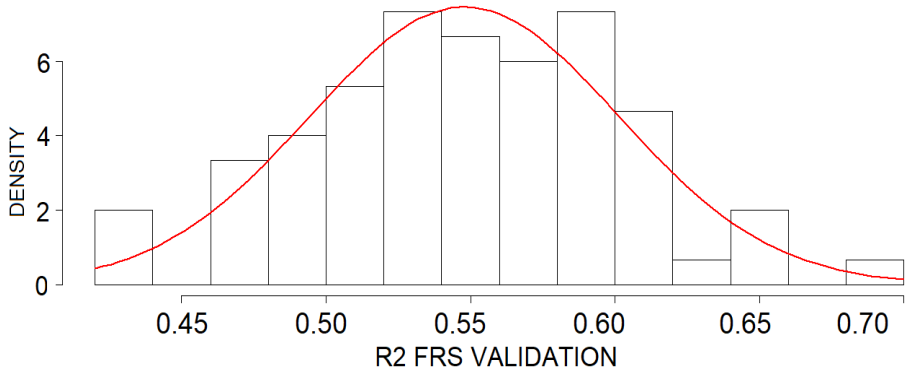

5.13(b): Validation phase with mean 0.54788858 and SD 0.05346327.

Figure 5.13: R^2 distribution for both FRS estimation and validation on 75 runs. Note that as R^2 only goes to a maximum value of 1, the fitted curve for the estimation is limited to it.

Part III

Conclusions

6
Final Considerations

The present work explored the application of SI methodology and black-box data-driven models in two applications of PEA: (i) micromanipulators and (ii) acoustic transmission. Different types of signals, preprocessing methods, and evaluation metrics were explored. All with experimental data, acquired through the use of specially developed test benches to mimic the real-world application.

Concerning the micromanipulators, it was shown that deep neural networks are feasible for dynamic modeling. Additionally, the importance of the use of a general-purpose excitation signal for acquiring data to create the model was demonstrated.

With respect to the acoustic transmission case, few works in the literature are found employing the SI methodology for this application of PEA. The results show the great potential of black-box models in comparison to analytical approach models, primarily when computational performance is important for monitoring, as environmental changes may take place. Several models, namely, linear ARMAX, power-form polynomial NARMAX models, and several thousand configurations of the NARX with ANN model structure were tested. In the specific case of the NARX-ANN models, although a perfect accuracy for the validation data was not achieved, it paves the way for further improvements as it serves as a proof of concept of the use of ANN for this specific application. Nevertheless, the models are useful for tracking time-varying systems at short prediction windows. This is extremely relevant since the optimal frequency response, which determines the maximum gain in transmission, can be influenced by the parameters of the obtained model. The mere fact that the methodologies here utilized require only input and output data is worth the effort.

Based on the contributions and its results, the following suggestions are made to further improve the models of piezoelectric in micromanipulation and acoustic transmission in future research:

– More research shall be diverted to the creation of a more automatic approach to generate models, such as the use of neuroevolution techniques [85]. It still lacks relevant engineering applications that involve

dynamic systems modeling such as monitoring, prediction, compensation, and simulation. Even if the use of such techniques implies greater computational burden, the combination of powerful complex representation and ease of model creation may play an important role in the nonlinear black-box system identification space as it is time-consuming and thus expensive to create models at scale, if not impossible, when problem-dependent decisions are needed.

– Further study is needed to comprehend how different assumptions and changes in the operational conditions affect the model performance. A few examples, in the case of the acoustic transmission, are the distance between the Rx and Tx PEA, the type of fluid, and its temperature. For the micromanipulator case, it is needed to study how pure sinusoidal with simultaneous different amplitudes and frequency affect the modeling and hysteresis loops.

– As the bandwidth and sampling frequency required by the piezoelectric here presented are large, new methods for handling big datasets are a handful for black-box modeling. The used methods cannot accommodate the several thousand samples, after preprocessing of the acquired data, simultaneously or in batch mode. As such, it is required to truncate the data leading to a potential loss of accuracy of the models.

– An expansion of the ANN model through the use of Recurring Neural Networks that have temporal dynamic behavior ("memory") or Physically Informed Artificial Networks, that takes into consideration physical laws described through the nonlinear partial differential, could lead to improvements and interesting results, especially in the acoustic transmission. Additionally, an ensemble of models shall be investigated for the micromanipulators as it may lead to a better fit as suggested when comparing the residuals in Figure 5.1.

– Improvements in the test bench to overcome limitations in the available hardware are needed. Those were circumvented in the present work, but future research could include the use of better and/or use of specifically made equipment/circuitry reducing the uncertainties introduced by the aforementioned circumvented limitations. This includes better signal generators that can fully utilize broadband signals, such as the multisine, with all its components. And, in the specific case of the acoustic transmission, a large tank or specialized circuitry to mitigate inner reflections that cross-feeds the PEA and contaminates the data. The use of equipment with high voltage data acquisition capabilities, to remove the

amplifier from the model, is not mandatory. In some real world applications, all the electronics needed for signal amplification and conditioning are not easily detached from the system and needs to be accounted for in the model.

– One shortcoming of the acoustic transmission approach here taken is the use of a single Tx and Rx. For the magnetic coupling approach of wireless power transfer, the authors in [59] say that the use of multiple-input single-output systems have increased power transfer when compared to the single-input single-output approach. However, at the same time, it poses new challenges for the modeling due to increased number of DOF. The acoustic approach may not be different once, by analogy with the magnetic coupling method, the increased number of Tx and/or Rx PEA introduces secondary reflections that lead to cross-feed and contaminate the data.

Bibliography

[1] JAFFE, B.. **Piezoelectric ceramics**, volumen 3. Elsevier, 2012.

[2] GU, G.-Y.; ZHU, L.-M.; SU, C.-Y.; DING, H. ; FATIKOW, S.. **Modeling and control of piezo-actuated nanopositioning stages: A survey**. IEEE Transactions on Automation Science and Engineering, 13(1):313–332, 2014.

[3] ADRIAENS, H.; DE KONING, W. L. ; BANNING, R.. **Modeling piezoelectric actuators**. IEEE/ASME transactions on mechatronics, 5(4):331–341, 2000.

[4] RAKOTONDRABE, M.. **Smart materials-based actuators at the micro/nano-scale. Characterization, Control and Applications**. Springer, 2013.

[5] DEVASIA, S.; ELEFTHERIOU, E. ; MOHEIMANI, S. R.. **A survey of control issues in nanopositioning**. IEEE Transactions on Control Systems Technology, 15(5):802–823, 2007.

[6] RAKOTONDRABE, M.. **Combining self-sensing with an unkown-input-observer to estimate the displacement, the force and the state in piezoelectric cantilevered actuator**. American Control Conference, 2013.

[7] ALJANAIDEH, O.; OTHERS. **Observer and robust h-inf control of a 2-dof piezoelectric actuator equipped with self-measurement**. IEEE Robotics Automation Letter, 3:1080-1087, 2018.

[8] IVAN, I. A.; OTHERS. **Quasi-static displacement self-sensing measurement for a 2-dof piezoelectric cantilevered actuator**. IEEE Transactions on Industrial Electronics, DOI.10.1109/TIE.2017.2677304, 2017.

[9] JANOCHA, H.; KUHNEN, K.. **Real-time compensation of hysteresis and creep in piezoelectric actuators**. Sensors and actuators A: Physical, 79(2):83–89, 2000.

[10] RAKOTONDRABE, M.. **Multivariable classical prandtl–ishlinskii hysteresis modeling and compensation and sensorless control of a nonlinear 2-dof piezoactuator**. Nonlinear Dynamics, 89(1):481–499, 2017.

[11] MIRI, N.; MOHAMMADZAHERI, M. ; CHEN, L.. **A comparative study of different physics-based approaches to modelling of piezoelectric actuators**. In: 2013 IEEE/ASME INTERNATIONAL CONFERENCE ON ADVANCED INTELLIGENT MECHATRONICS, p. 1211–1216. IEEE, 2013.

[12] HABINEZA, D.; OTHERS. **Multivariable generalized bouc-wen modeling, identification and feedforward control and its application to a 2-dof piezoelectric multimorph actuator**. IFAC WC, 10952-10958, 2014.

[13] DENG, L.; TAN, Y.. **Modeling hysteresis in piezoelectric actuators using narmax models**. Sensors and Actuators A: Physical, 149(1):106–112, 2009.

[14] TANGIRALA, A. K.. **Principles of system identification: theory and practice (1st ed.)**. Crc Press, 2015.

[15] SAAD, M. S.; JAMALUDDIN, H. ; DARUS, I. Z. M.. **Active vibration control of a flexible beam using system identification and controller tuning by evolutionary algorithm**. Journal of Vibration and Control, 21(10):2027–2042, 2015.

[16] LOU, J.; LIAO, J.; WEI, Y.; YANG, Y. ; LI, G.. **Experimental identification and vibration control of a piezoelectric flexible manipulator using optimal multi-poles placement control**. Applied Sciences, 7(3):309, 2017.

[17] LENNART, L.. **System identification: theory for the user**. PTR Prentice Hall, Upper Saddle River, NJ, 28, 1999.

[18] KEESMAN, K. J.. **System identification: an introduction**. Springer Science & Business Media, 2011.

[19] SETHI, S. P.; THOMPSON, G. L.. **What is optimal control theory?** Springer, 2000.

[20] BEKEY, G. A.; BENEKEN, J. E.. **Identification of biological systems: a survey**. Automatica, 14(1):41 – 47, 1978.

[21] ZHAO, Y.; WESTWICK, D. T. ; KEARNEY, R. E.. **Subspace methods for identification of human ankle joint stiffness**. IEEE transactions on biomedical engineering, 58(11):3039–3048, 2010.

[22] HAHN, J.-O.; MCCOMBIE, D. B.; REISNER, A. T.; HOJMAN, H. M. ; ASADA, H. H.. **Identification of multichannel cardiovascular dynamics using dual laguerre basis functions for noninvasive cardiovascular monitoring**. IEEE Transactions on Control Systems Technology, 18(1):170–176, 2009.

[23] HAJIZADEH, I.; OTHERS. **Multivariable recursive subspace identification with application to artificial pancreas systems**. IFAC WC, 50(1):886 – 891, 2017.

[24] ABDELHADY, M.; OTHERS. **System identification and control optimization of an active prosthetic knee in swing phase**. American Control Conf, p. 857–862, 2017.

[25] BECK, M.. In: HVDROLOGICAL FORECASTING-PRÉVISIONS HYDROLOGIQUES, volumen 129 de **Proceedings of the Oxford Symposium**, p. 123–131. Int Association of Hydrological Science, April 1980.

[26] EVSUKOFF, A. G.; DE LIMA, B. S. ; EBECKEN, N. F.. **Long-term runoff modeling using rainfall forecasts with application to the iguaçu river basin**. Water resources management, 25(3):963–985, 2011.

[27] BILLINGS, S. A.. **Nonlinear system identification: NARMAX methods in the time, frequency, and spatio-temporal domains**. John Wiley & Sons, 2013.

[28] YU, S.; ALICI, G.; SHIRINZADEH, B. ; SMITH, J.. **Sliding mode control of a piezoelectric actuator with neural network compensating rate-dependent hysteresis**. In: PROCEEDINGS OF THE 2005 IEEE INTERNATIONAL CONFERENCE ON ROBOTICS AND AUTOMATION, p. 3641–3645. IEEE, 2005.

[29] CHENG, L.; LIU, W.; HOU, Z.-G.; YU, J. ; TAN, M.. **Neural-network-based nonlinear model predictive control for piezoelectric actuators**. IEEE Transactions on Industrial Electronics, 62(12):7717–7727, 2015.

[30] SONG, D.; LI, C. J.. **Modeling of piezo actuator's nonlinear and frequency dependent dynamics**. Mechatronics, 9(4):391–410, 1999.

[31] DONG, X.-J.; MENG, G. ; PENG, J.-C.. **Vibration control of piezoelectric smart structures based on system identification technique: Numerical simulation and experimental study**. Journal of sound and vibration, 297(3-5):680–693, 2006.

[32] AYALA, H. V. H.; HABINEZA, D.; RAKOTONDRABE, M.; KLEIN, C. E. ; COELHO, L. S.. **Nonlinear black-box system identification through neural networks of a hysteretic piezoelectric robotic micromanipulator**. IFAC-PapersOnLine, 48(28):409–414, 2015.

[33] AYALA, H. V. H.; RAKOTONDRAHE, M. ; DOS SANTOS COELHO, L.. **Modeling of a 2-dof piezoelectric micromanipulator at high frequency rates through nonlinear black-box system identification**. In: 2018 ANNUAL AMERICAN CONTROL CONFERENCE (ACC), p. 4354–4359. IEEE, 2018.

[34] OUYANG, P.; ZHANG, W.; GUPTA, M. M. ; ZHAO, W.. **Overview of the development of a visual based automated bio-micromanipulation system**. Mechatronics, 17(10):578–588, 2007.

[35] KEEKYOUNG KIM; XINYU LIU; YONG ZHANG ; YU SUN. **Micronewton force-controlled manipulation of biomaterials using a monolithic mems microgripper with two-axis force feedback**. In: 2008 IEEE INTERNATIONAL CONFERENCE ON ROBOTICS AND AUTOMATION, p. 3100–3105, 2008.

[36] HEPING CHEN; NING XI ; GUANGYONG LI. **Cad-guided automated nanoassembly using atomic force microscopy-based nonrobotics**. IEEE Transactions on Automation Science and Engineering, 3(3):208–217, 2006.

[37] SALAPAKA, S. M.; SALAPAKA, M. V.. **Scanning probe microscopy**. IEEE Control Systems Magazine, 28(2):65–83, 2008.

[38] HUBBARD, N. B.; CULPEPPER, M. L. ; HOWELL, L. L.. **Actuators for Micropositioners and Nanopositioners**. Applied Mechanics Reviews, 59(6):324–334, 11 2006.

[39] NIEZRECKI, C.; BREI, D.; BALAKRISHNAN, S. ; MOSKALIK, A.. **Piezoelectric actuation: state of the art**. 2001.

[40] ESCARENO, J.; RAKOTONDRABE, M. ; HABINEZA, D.. **Backstepping-based robust-adaptive control of a nonlinear 2-dof piezoactuator**. Control Engineering Practice, 41:57–71, 2015.

[41] NARENDRA, K. S.; PARTHASARATHY, K.. **Identification and control of dynamical systems using neural networks**. IEEE Trans on Neural Networks, 1:4–27, 1990.

[42] AYALA, H. V. H.; DOS SANTOS COELHO, L.. **Cascaded evolutionary algorithm for nonlinear system identification based on correlation functions and radial basis functions neural networks**. Mechanical Systems and Signal Processing, 68-69:378 – 393, 2016.

[43] LI, X.; YU, W.. **Dynamic system identification via recurrent multilayer perceptrons**. Information Sciences, 147(1):45 – 63, 2002.

[44] LECUN, Y.; BENGIO, Y. ; HINTON, G.. **Deep learning**. Nature, 521(7553):436, 2015.

[45] DE LA ROSA, E.; YU, W.. **Randomized algorithms for nonlinear system identification with deep learning modification**. Information Sciences, 364, 2016.

[46] BOX, G. E. P.; JENKINS, G. M.. **Time series analysis, forecasting and control**. Holden Day, San Francisco, USA, 1970.

[47] NARENDRA, K. S.; PARTHASARATHY, K.. **Gradient methods for the optimization of dynamical systems containing neural networks**. IEEE Transactions on Neural Networks, 2(2):252–262, March 1991.

[48] SCHOUKENS, M.; NOEL, J.. **Three benchmarks addressing open challenges in nonlinear system identification**. IFAC WC, p. 446 – 451, 2017.

[49] QIAO, J.; OTHERS. **A deep belief network with PLSR for nonlinear system modeling**. Neural Networks, 104:68–79, 2018.

[50] TAKAHASHI, V. L.; KUBRUSLY, A. C.; BRAGA, A.; QUINTERO, S. M.; FIGUEIREDO, S. W. ; DOMINGUES, A. B.. **Ultrasonic power and data transfer through multiple curved layers applied to pipe instrumentation**. Sensors, 19(19):4074, 2019.

[51] YANG, D.-X.; HU, Z.; ZHAO, H.; HU, H.-F.; SUN, Y.-Z. ; HOU, B.-J.. **Through-metal-wall power delivery and data transmission for enclosed sensors: A review**. Sensors, 15(12):31581–31605, 2015.

[52] SHOUDY, D.; SAULNIER, G.; SCARTON, H.; DAS, P.; ROA-PRADA, S.; ASHDOWN, J. ; GAVENS, A.. **P3f-5 an ultrasonic through-wall**

communication system with power harvesting. In: 2007 IEEE ULTRASONICS SYMPOSIUM PROCEEDINGS, p. 1848–1853. IEEE, 2007.

[53] GRAHAM, D. J.; NEASHAM, J. A. ; SHARIF, B. S.. **Investigation of methods for data communication and power delivery through metals**. IEEE Transactions on industrial electronics, 58(10):4972–4980, 2011.

[54] HU, Y.; ZHANG, X.; YANG, J. ; JIANG, Q.. **Transmitting electric energy through a metal wall by acoustic waves using piezoelectric transducers**. IEEE Transactions on Ultrasonics, Ferroelectrics, and Frequency Control, 50(7):773–781, 2003.

[55] HU, H.; HU, Y.; CHEN, C. ; WANG, J.. **A system of two piezoelectric transducers and a storage circuit for wireless energy transmission through a thin metal wall**. IEEE transactions on ultrasonics, ferroelectrics, and frequency control, 55(10):2312–2319, 2008.

[56] KLUGE, M.; BECKER, T.; SCHALK, J. ; OTTERPOHL, T.. **Remote acoustic powering and data transmission for sensors inside of conductive envelopes**. In: SENSORS, 2008 IEEE, p. 41–44. IEEE, 2008.

[57] CHAKRABORTY, S.; WILT, K. R.; SAULNIER, G. J.; SCARTON, H. A. ; DAS, P. K.. **Estimating channel capacity and power transfer efficiency of a multi-layer acoustic-electric channel**. In: WIRELESS SENSING, LOCALIZATION, AND PROCESSING VIII, volumen 8753, p. 87530F. International Society for Optics and Photonics, 2013.

[58] LAWRY, T. J.; WILT, K. R.; SCARTON, H. A. ; SAULNIER, G. J.. **Analytical modeling of a sandwiched plate piezoelectric transformer-based acoustic-electric transmission channel**. IEEE transactions on ultrasonics, ferroelectrics, and frequency control, 59(11):2476–2486, 2012.

[59] CHEN, F.; YOUNG, P. C.; GARNIER, H.; DENG, Q. ; KAZIMIERCZUK, M. K.. **Data-driven modeling of wireless power transfer systems with multiple transmitters**. IEEE Transactions on Power Electronics, 35(11):11363–11379, 2020.

[60] CHEN, F.; PADILLA, A.; YOUNG, P. C. ; GARNIER, H.. **Data-driven modeling of wireless power transfer systems with slowly time-varying parameters**. IEEE Transactions on Power Electronics, 35(11):12442–12456, 2020.

[61] NOEL, J.; ESFAHANI, A.; KERSCHEN, G. ; SCHOUKENS, J.. **A nonlinear state-space approach to hysteresis identification**. Mechanical Systems and Signal Processing, 84:171 – 184, 2017.

[62] NØRGÅRD, P. M.; RAVN, O.; POULSEN, N. K. ; HANSEN, L. K.. **Neural networks for modelling and control of dynamic systems: a practitioner's handbook**. Springer-Verlag, London, 2000.

[63] LAI, E.. **2 - converting analog to digital signals and vice versa**. In: Lai, E., editor, PRACTICAL DIGITAL SIGNAL PROCESSING, p. 14 – 49. Newnes, Oxford, 2003.

[64] LJUNG, L.. **Perspectives on system identification**. Annual Reviews in Control, 34(1):1–12, 2010.

[65] PINTELON, R.; SCHOUKENS, J.. **System identification: a frequency domain approach**. John Wiley & Sons, 2012.

[66] SCHOUKENS, J.; PINTELON, R. ; ROLAIN, Y.. **Mastering system identification in 100 exercises**. John Wiley & Sons, 2012.

[67] SCHROEDER, M.. **Synthesis of low-peak-factor signals and binary sequences with low autocorrelation (corresp.)**. IEEE Transactions on Information Theory, 16(1):85–89, 1970.

[68] LJUNG, L.. **Black-box models from input-output measurements**. In: IMTC 2001. PROCEEDINGS OF THE 18TH IEEE INSTRUMENTATION AND MEASUREMENT TECHNOLOGY CONFERENCE. REDISCOVERING MEASUREMENT IN THE AGE OF INFORMATICS (CAT. NO. 01CH 37188), volumen 1, p. 138–146. IEEE, 2001.

[69] BOHLIN, T. P.. **Practical grey-box process identification: theory and applications**. Springer Science & Business Media, 2006.

[70] KRISTENSEN, N. R.; MADSEN, H. ; JØRGENSEN, S. B.. **Parameter estimation in stochastic grey-box models**. Automatica, 40(2):225–237, 2004.

[71] AYALA, H. V. H.; GRITTI, M. C. ; DOS SANTOS COELHO, L.. **An r library for nonlinear black-box system identification**. SoftwareX, 11:100495, 2020.

[72] HAYKIN, S. S.; OTHERS. **Neural networks and learning machines/simon haykin.**, 2009.

[73] CHEN, S.; BILLINGS, S.. **Neural networks for nonlinear dynamic system modelling and identification**. International journal of control, 56(2):319–346, 1992.

[74] GOODFELLOW, I.; BENGIO, Y.; COURVILLE, A. ; BENGIO, Y.. **Deep learning**, volumen 1. MIT press Cambridge, 2016.

[75] GLOROT, X.; BORDES, A. ; BENGIO, Y.. **Deep sparse rectifier neural networks**. In: PROCEEDINGS OF THE FOURTEENTH INTERNATIONAL CONFERENCE ON ARTIFICIAL INTELLIGENCE AND STATISTICS, p. 315–323. JMLR Workshop and Conference Proceedings, 2011.

[76] AHMAD, R.; JAMALUDDIN, H.. **Orthogonal least square algorithm and its application for modelling suspension system**. Jurnal Teknologi, 34(1):71–84, 2001.

[77] GOODFELLOW, I.; BENGIO, Y. ; COURVILLE, A.. **Deep learning**. MIT press, 2017.

[78] HINTON, G.. **Neural networks for machine learning**, 2012.

[79] TIELEMAN, T.; HINTON, G.. **Lecture 6.5-rmsprop: Divide the gradient by a running average of its recent magnitude**. COURSERA: Neural networks for machine learning, 4(2):26–31, 2012.

[80] BENGIO, Y.; CA, M.. **Rmsprop and equilibrated adaptive learning rates for nonconvex optimization**. corr abs/1502.04390, 2015.

[81] BLLLINGS, S.; VOON, W.. **Correlation based model validity tests for non-linear models**. International journal of Control, 44(1):235–244, 1986.

[82] BILLINGS, S.; JAMALUDDIN, H. ; CHEN, S.. **Properties of neural networks with applications to modelling non-linear dynamical systems**. International Journal of Control, 55(1):193–224, 1992.

[83] AGUIRRE, L. A.. **A Bird's Eye View of Nonlinear System Identification**. arXiv e-prints, p. arXiv:1907.06803, Jul 2019.

[84] CHOLLET, F.; OTHERS. **Keras: Deep learning library for theano and tensorflow**. URL: https://keras. io/k, 7(8):T1, 2015.

[85] STANLEY, K. O.; CLUNE, J.; LEHMAN, J. ; MIIKKULAINEN, R.. **Designing neural networks through neuroevolution**. Nature Machine Intelligence, 1(1):24–35, 2019.